Symmetry in frontal but not motor and somatosensory corticocortical and corticostriatal circuitry

Abbreviated title: Corticocortical and corticostriatal symmetry

Andrew E. Papale[4], Madhumita Harish[2], Ronald F. Paletzki[1], Nathan J. O'Connor[3], Brian S. Eastwood[3], Rebecca P. Seal[2], Ross S. Williamson[2], Charles R. Gerfen[1*], Bryan M. Hooks[2*]

[1]Laboratory of Systems Neuroscience, NIMH, Bethesda, MD
[2]Department of Neurobiology, University of Pittsburgh School of Medicine, Pittsburgh, PA
[3]MBF Bioscience, Williston, VT
[4]Department of Psychiatry, University of Pittsburgh School of Medicine, Pittsburgh, PA

[*]Corresponding authors: hooksm@pitt.edu (BMH); gerfenc@mail.nih.gov (CRG)

Correspondence: Dr. Bryan M. Hooks, 200 Lothrop Street BSTWR Suite W1458
Pittsburgh, PA 15213; 412-624-8465; hooksm@pitt.edu

Number of pages: 28
Number of figures: 8 (Two extended data figures)
Number of tables: 1
Words for abstract (179), significance (119), introduction (748), and discussion (1831)

Conflict of interest statement: The authors declare no competing financial interests.

Acknowledgements: We thank Afonso Silva, Rob Turner, Andreea Bostan, and members of the Hooks lab for comments and suggestions. We thank Jack Glaser, Paul Angstman, Sue Tappan, Mike Fay and Scott Gerfen at MBF Bioscience for the collaboration to develop and use the BrainMaker software. This work was supported by a NARSAD Young Investigator Award (BMH), NIH NINDS R01 NS103993 (BMH), a CDMRP PRMRP Discovery Award PR201842 (BMH), a Whitehall Foundation award (BMH), and a National Institute of Mental Health IRP award (ZIA MH002497-33) to C.R.G.

Author contributions: A.E.P, B.M.H., and C.R.G. conceived of the project and analyzed the data. A.E.P, M.H., N.J.O., and B.S.E. developed software for analyzing the data. R.F.P. and C.R.G. sectioned and imaged the tissue. B.M.H., A.E.P., R.S.W., R. P. S., and C.R.G wrote the paper with help from all authors.

Abstract

Neocortex and striatum are topographically organized by cortical areas representing sensory and motor functions, where primary cortical areas are generally used as models for other cortical regions. But different cortical areas are specialized for distinct purposes, with sensory and motor areas lateralized for touch and motor control, respectively. Frontal areas are involved in decision making, where lateralization of function may be less important. This study contrasted the topographic precision of ipsilateral and contralateral projections from cortex based on the injection site location. While sensory cortical areas had strongly topographic outputs to ipsilateral cortex and striatum, they were weaker and not as topographically strong to contralateral targets. Motor cortex had somewhat stronger projections, but still relatively weak contralateral topography. In contrast, frontal cortical areas had high degrees of topographic similarity for both ipsilateral and contralateral projections to cortex and striatum. This contralateral connectivity reflects on the pathways in which corticostriatal computations might integrate input outside closed basal ganglia loops, enabling the two hemispheres to act as a single unit and converge on one result in motor planning and decision making.

(Word count: 179)

Significance Statement

The mammalian brain is divided into two cerebral hemispheres, each responsible for sensation and movement on the opposite side of the body. The two sides communicate via an enormous bundle of midline-crossing fibers, the corpus callosum. The callosal projections mainly target neocortex and striatum. While callosal projections originate from most areas of the neocortex, how the anatomy and function of these projections might vary across motor, sensory, and frontal regions is unknown. In particular, callosal projections are proposed here to play a large role in frontal areas, where maintaining unity across hemispheres in value assessment and decision-making for the whole individual is key, but a smaller role for sensory representations where perceptions from the contralateral body are less informative.

(Word count: 119)

Introduction

Somatotopic organization of primary motor (M1) and primary somatosensory (S1) areas of cerebral cortex have been long established by stimulation(Penfield and Boldery, 1937) since first being predicted by the march of seizures through adjacent body parts(York and Steinberg, 2011). This principle extends to other primary sensory areas, including visual cortex(Drager, 1975) and auditory cortex(Merzenich and Brugge, 1973; Morel et al., 1993), with topography maintained in some higher order areas pertaining to sensation (Carvell and Simons, 1986; Felleman and Van Essen, 1991; Wang and Burkhalter, 2007). But the criteria for topographic organization in decision-making areas is less clear. Quantification of the precision of somatotopic organization in an area has been a challenge in motor areas. Microstimulation methods used to quantify motor somatotopy vary in precision with threshold current used(Tennant et al., 2011) and current spread during stimulation(Histed et al., 2012). Anatomical methods relying on bulk injections lose precision as tracer or virus at the injection site spreads (Bohland et al., 2009; Oh et al., 2014; Zingg et al., 2014).

Corticocortical projections connect cortical areas to higher and lower order regions processing similar information, such as from S1 to secondary somatosensory cortex (S2), as well as across modalities, as from S1 to M1, though both of these projections show characteristics suggesting precise topography is not maintained: The S1 to S2 projection is anisotropic, favoring integration across whisker rows(Hoffer et al., 2003), while the S1 to M1 projection is elongated across a broad anterior-posterior swath of M1(Mao et al., 2011; Rocco-Donovan et al., 2011). The laminar organization of such projections also varies, with projections from lower order to higher order areas typically originating in deeper layers and targeting upper ones, while higher order feedback often originates from upper layers and targets deeper ones (Felleman and Van Essen, 1991; Hooks, 2017; Hooks et al., 2013). These areas also send projections across the midline to the corresponding contralateral cortex (Brown and Hestrin, 2009; Petreanu et al., 2007). The density of this projection (and the size of the corpus callosum itself) suggests an important role in coordinating perception and movement.

Corticostriatal projections are topographically organized, but cortical output from any given cortical area projects somewhat broadly, overlapping with the output from other cortical areas(Alloway et al., 2000; Hintiryan et al., 2016). These projections originate mainly from layer 5, with some contribution from layer 2/3(McGeorge and Faull, 1989). Striatal regions integrate input from functionally related cortical areas. The main features are the convergence of excitatory cortical (and some thalamic) input from a large number of afferents onto the striatal projection neurons (SPNs) in striatum, which in turn project either in the indirect pathway (to external globus pallidus) or the direct pathway (to substantia nigra pars reticulata and internal globus pallidus/entopeduncular nucleus), with some convergence onto a smaller number of neurons at each step, eventually outputting to thalamus and brainstem(Lee et al., 2020). A major organizational feature of these projections is that they form loops from cortex through basal ganglia and thalamus that are largely parallel and functionally segregated(Alexander et al., 1986). These loops include inputs from related cortical areas(Middleton and Strick, 2000). These areas may be reciprocally connected, as somatotopically congruent regions of M1 and S1 (Alloway et al., 2006; Hooks et al., 2018) or grasp-related regions across the cortex(Gerbella et al., 2016), but also include non-connected cortical areas(Choi et al., 2017; Selemon and Goldman-Rakic, 1985). These loops are not exclusively concerned with motor control, but perform similar computations on incoming cortical information from frontal, premotor, motor, and temporal inputs (Middleton and Strick, 2000). Thus, these loops are called “globally parallel” but locally overlapping”(Haber, 2003; Jarbo and Verstynen, 2015).

Striatal input in non-human primate is dominated by ipsilateral input. There is not strong evidence for left/right asymmetry in ipsilateral corticostriatal projections(McGuire et al., 1991a; b). Unlike thalamostriatal input, which is exclusively ipsilateral, some cortical areas send contralateral projections, including parietal, motor, and frontal areas (Alloway *et al.*, 2006; Borra

et al., 2022; Jones et al., 1977; Kunzle, 1975; McGuire *et al.*, 1991b). Nevertheless, corticocortical and corticostriatal projections are organized and repeatable across animals(Hintiryan *et al.*, 2016; Zingg *et al.*, 2014). And, as with ipsilateral projections, there is overlap of striatal targeting from related cortical areas. By registering brains to a common coordinate system(Wang et al., 2020), comparisons of topographic organization across sensory and motor projections to striatum are possible, demonstrating an anatomical basis for higher somatotopic precision in sensory versus motor areas(Hooks *et al.*, 2018). Here, this comparison is extended to contralateral cortex and striatum.
(Word count: 748)

Methods

Injections

Surgical and experimental procedures conformed to National Institutes of Health guidelines for mice and were approved by the Institutional Animal Care and Use Committees of University of Pittsburgh and Janelia Research Campus. Tlx3_PL56 mice (N=33) from the GENSAT BAC Cre-recombinase driver line were used to trace corticocortical and corticostriatal projections. Mice of both sexes were injected at postnatal day ~P35 and sacrificed after 2-3 weeks of expression. Stereotaxic injections targeted the left hemisphere, with injection sites covering frontal, motor, and somatosensory. Injections in other cortical areas were excluded. 30 nL per injection site of AAV-flex-XFPs were injected at each of two cortical depths (~0.5 and 0.8 mm) using a custom positive displacement injector via a pulled borosilicate glass micropipette (Hooks *et al.*, 2018). The generic AAV-flex-XFP refers to several tracing viruses used (see Table 1), including EGFP, tdTomato, and mRuby2-based spaghetti monster fluorescent proteins (smFPs)(Viswanathan et al., 2015).

Histology, staining, and imaging

Mice were transcardially perfused with phosphate-buffered saline (PBS) followed by 4% paraformaldehyde in PBS and postfixed overnight. Brains were then transferred to 20% sucrose in PBS. Brains were sectioned at 80 µm. EGFP, tdTomato, and smFPs were immunoamplified. Neurotrace Blue (1:100) was used as a structural marker for alignment and registration. Sections were imaged using Neurolucida (v2017, MBF Bioscience, Williston, VT) on a Zeiss Axioimager (Zeiss, Oberkochen, Germany) equipped with 10x objective, Ludl motorized stage and a Hamamatsu Orca Flash 4.0 camera (Hamamatsu, Hamamatsu City, Japan). Brain sections were tiled images of the average of ~100-200 tiles. Each tile consisted of image stacks collected in 10 µm steps. A single 3D image was first generated and images were collapsed to a single plane using a DeepFocus algorithm implemented in Neurolucida(Gerfen et al., 2013; Paletzki and Gerfen, 2015).

Whole brain reconstruction, annotation, and registration

Stacks of brain images were aligned to a standard coordinate system using BrainMaker software (MBF Bioscience, Williston, VT) as previously described(Eastwood et al., 2019; Tappan et al., 2019). Briefly, serially-reconstructed brains contained 10 µm isotropic voxels (782x1086x1242) and were registered to the annotated Allen Mouse Common Coordinate Framework (CCFv3; http://connectivity.brain-map.org) (Wang *et al.*, 2020). Neurotrace Blue was used as the structural marker for registration. This required a two-stage registration process. The first stage constructed an average reference space from NeurotraceBlue images (the average of brains sectioned, mounted, and stained with Neurotrace Blue; 78 individual brains). Multiple resolution registration optimized 12 parameters of a 3D affine transform to minimize a normalized correlation metric between each brain and the template image. The reference template was then updated by resampling all individual brains with their respective affine transforms and computing a voxel-wise weighted average. A second pass registered each

individual brain to the new template, updating the individual transforms. This process repeated until the template image stabilized. The second stage registered the average reference image to the Allen CCFv3 (based on 1675 brains visualized with 2--photon auto-fluorescence (Kuan et al., 2015)). 300 unique landmarks were identified and positions of the landmarks were used to construct a nonlinear transform that models deformation of a uniform mesh grid with B-splines. The result is an average reference image and its spatially aligned annotation volume that constitutes the average reference atlas. Individual brains here were registered using NeurotraceBlue with the average reference space by adjusting parameters of a 3D affine and 3D nonlinear B-spline transform to minimize a normalized correlation metric.

For quantification of injection site location, tiled images were imported into Neurolucida software (MBF Bioscience, Williston, VT) and soma locations were annotated using automated object detection with manual supervision. Nearest neighbor interpolation of the average reference space volume at the mapped positions provided the anatomical region assignment for each cell. Coordinates of the CCFv3 for structures of interest (cortex and striatum) were used to identify voxels for quantification. These were divided into left and right hemispheres to distinguish ipsilateral and contralateral sides.

Data analysis

Aligned brain images were downsampled to 50 µm isotropic voxels (156x217x248) using custom routines in FIJI software62. The annotated Allen Mouse CCF was also used at 10 µm and downsampled to 50 µm. The annotation was used to assign voxels to a given brain region (ipsilateral or contralateral striatum, for example). Both 10 µm and 50 µm images were converted from tifs into .mat files in Matlab (Mathworks, Natick, MA) for analysis with custom routines. Soma locations were similarly imported to Matlab. Differences in voxel intensity and the intensity ratio between ipsi- and contralateral sides (Fig. 3E-F and Fig. 7E-F) were tests by one way ANOVA followed up by Tukey-corrected pairwise t-tests. Differences in the correlation (versus injection site offset, Fig. 3G-I and Fig. 7G-I) were assessed by two way ANCOVA to examine the effects of region and ipsi/contra target sites on correlations (PCC), after controlling for distance. Since there was a statistically significant two-way interaction, a follow up analysis of was performed with Bonferroni correction.

Data availability statement

The data and images used in this study are available upon request. Aligned images in 10 and 50 µm voxels for all brains, cell soma locations, and the corresponding masks used to identify brain regions (striatum and cortex) are available on request as well as the custom Matlab code used for data analysis. Original images of whole brains are freely available online at http://gerfenc.biolucida.net/link?l=Jl1tV7.

Table 1 | Viral reagents for tracing

Construct name	Addgene number	Addgene name
AAV2/1-CAG-flex-EGFP	51502	pCAG-FLEX-EGFP-WPRE
AAV2/1-CAG-flex-tdTomato	51503	pCAG-FLEX-tdTomato-WPRE
AAV2/1-CAG-flex-GFPsmFP-FLAG	59756	pCAG-smFP-FLAG
AAV2/1-CAG-flex-GFPsmFP-Myc	59757	pCAG-smFP-Myc
AAV2/1-CAG-flex-GFPsmFP-V5	59758	pCAG-smFP-V5
AAV2/1-CAG-flex-GFPsmFP-HA	59759	pCAG-smFP-HA
AAV2/1-CAG-flex-mRuby2smFP-FLAG	59760	pCAG-mRuby2-smFP-FLAG
AAV2/1-CAG-flex-mRuby2smFP-OLLAS	59761	pCAG-mRuby2-smFP-OLLAS

Results

Examining a dense database of crossed corticocortical and corticostriatal projections

Neocortical layer 5 (L5) contains two main projection neuron types, intratelencephalic (IT-type) and pyramidal tract type (PT-type). IT-type neurons project to both ipsi- and contralateral cortex and striatum. To generate the image database(Hooks *et al.*, 2018), a Cre-driver mouse line selective for IT-type neurons(Gerfen *et al.*, 2013) was injected with AAV expressing Cre-dependent tracers, including GFP, td-tomato, and smFPs (Table 1) (Viswanathan *et al.*, 2015). Injections were made in a range of locations, including frontal, motor, and somatosensory cortex (Fig. 1). Each brain was reconstructed from tiled fluorescence images (Paletzki and Gerfen, 2015). These were registered to the Allen Common Coordinate Framework (CCFv3) (Wang *et al.*, 2020) using BrainMaker software (MBF Bioscience). Alignment precision was about ~50-70 µm(Hooks *et al.*, 2018). Placing all voxels and detected objects, such as somata, in a common coordinate space enabled quantitative comparisons of brain regions across different animals. The original images are freely available online at: http://gensatcrebrains.biolucida.net/images/?page=images&selectionType=collection&selectionId=32 (web-based) or can be viewed using the free downloaded Biolucida viewer software at: http://gerfenc.biolucida.net/link?l=JI1tV7.

Each injection was quantified in two ways. The first relied on detected cell bodies at the injection site. Injection site location was quantified as the center of mass of all infected somata. The somata of L5 IT-type neurons were detected and marked in Neurolucida. Their relative laminar depth was largely restricted to L5 (Fig. 1A-C), though a small number of L2/3 neurons could be seen, which was greatest in somatosensory injections (Fig, 1E). The injection site center of mass was calculated in coordinates registered to the Allen CCFv3, and plotted from a dorsal viewpoint (Fig.1D). The location was used to cluster injection sites into frontal (red), motor (purple), and somatosensory (blue)(Hooks *et al.*, 2018). This clustering corresponded well to existing division of the neocortex(Oh *et al.*, 2014; Zingg *et al.*, 2014) into primary somatosensory (SSp), primary motor (MOp), and secondary motor (MOs) regions. Furthermore, motor and frontal areas correspond to low threshold regions for evoking somatotopically organized body movements in rodent neocortex (Brecht et al., 2004; Hooks et al., 2011; Li and Waters, 1991; Tennant *et al.*, 2011). Injection sites could be further subdivided within general areas into subdivisions, such as whisker, forelimb, and orofacial regions of primary somatosensory cortex (vS1, fS1, and orfS1) which correspond to the CCFv3 regions

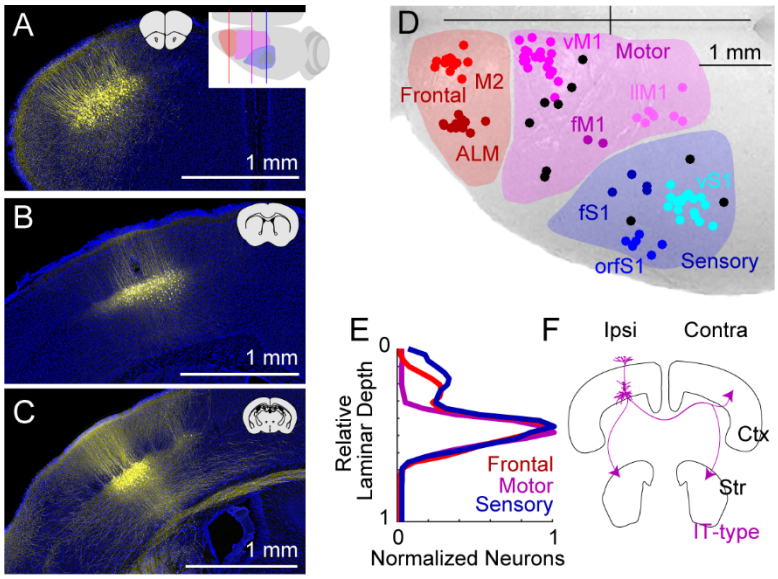

Figure 1 | Mapping layer 5 corticostriatal output from sensory and motor cortex

Injection site of AAV-DIO-XFP into frontal (A), motor (B), and sensory cortex (C) of Tlx3_PL56-Cre+ mice. Inset of coronal brain slices shows approximate location. In (A), top-down cartoon shows approximate planes of section. (D) Center of mass of all injection sites in sensory (blue, N=27), motor (purple, N=30), and frontal (red, N=25) cortex. Subdivisions within areas (M2, ALM, vM1, fM1, lIM1, vS1, fS1, and orfS1) are indicated in different colors, with uncategorized injection sites in black. Bregma is indicated as the cross at top right. (E) Quantification of relative depth of labeled Cre+ cortical neurons in frontal (red), motor (purple), and sensory (blue) cortex. (F) Cartoon of output targets of IT-type neurons.

SSp-bfd, SSp-ul, and SSp-n. Motor subdivisions (whisker, forelimb, and lower limb: vM1, fM1, lIM1) were also made, consistent with microstimulation maps and previous analysis of the injection sites(Hooks *et al.*, 2018). Frontal injections targeted the more medial M2(Hooks *et al.*, 2013) and the more lateral ALM(Komiyama et al., 2010). These did not correspond to subregions within the CCFv3 because the primary and secondary motor areas MOp and MOs are not somatopically divided in that atlas.

The second quantification of each injection compared projections from these injection sites. Thus, this relies on detecting suprathreshold axonal fluorescence from injections. A threshold was applied to aligned images to eliminate 99% of background voxels in target

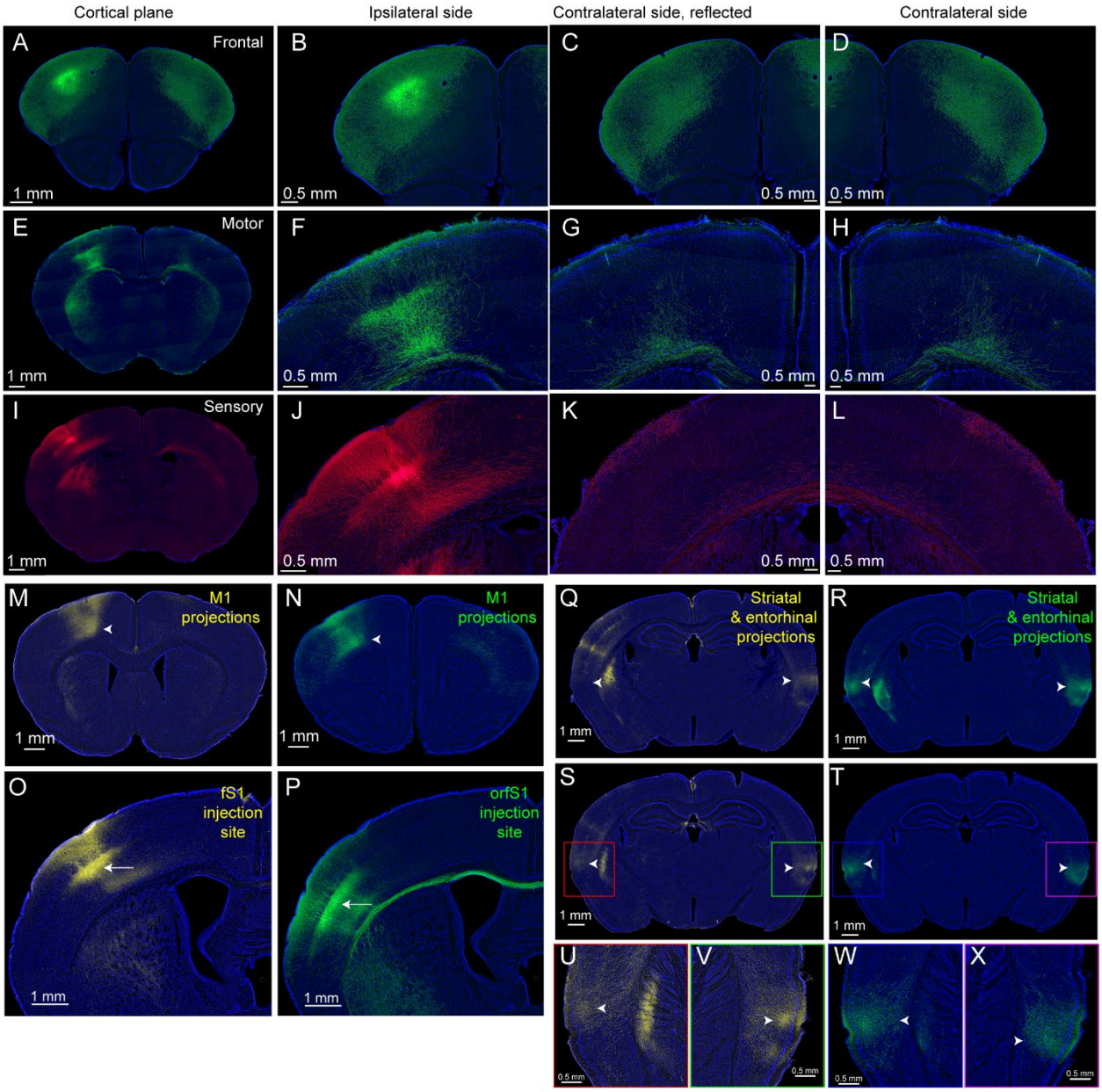

Figure 2 | Ipsi- and contralateral projections of IT-type neurons in frontal, motor, and somatosensory cortex
(A-D) Coronal images showing injection site of AAV-DIO-XFP into frontal cortex (ALM), with ipsi- (B) and contralateral (D) cortex presented for comparison. Reflected image of contralateral side (C) shown for comparison. (E-H) Similar presentation for motor cortex (fM1) injection. (I-L) Similar presentation for somatosensory cortex (vS1) injection. (M-X) Comparisons of projections from different regions within S1. (M-N) M1 projections from fS1 (yellow) and orfS1 (green). (O-P) Injection sites. (Q-X) Striatal and entorhinal projections, with higher resolution images (U-X). Arrows show cell bodies; arrowheads show axonal projections.

regions where no IT-type projections were expected (thalamus and hippocampus) for the fluorescence channel associated with a given injection. Aligned images are presented throughout using 50 μm-size voxels (50 μm x 50 μm x 50 μm).

High correlation of projection targeting in corticocortical projections

IT-type neurons project to four major regions: ipsilateral and contralateral cortex and ipsilateral and contralateral striatum (Fig. 1F). Some individual IT-type neurons collateralize to all four areas, while others show different patterns(Economo et al., 2016; Winnubst et al., 2019). These projections to both cortex and striatum suggest two straightforward comparisons across the midline. Examination of contralateral corticocortical projections suggests differences in the symmetry of these projections across the surface of cortex (Fig. 2). Frontal cortex injections had relatively strong axonal fluorescence in contralateral cortex (Fig. 2A-D), while this fluorescence became weaker in motor injections (Fig. 2E-H) and weaker still in somatosensory ones (Fig. 2I-L). This is not because somatosensory neurons are incapable of making long-range projects, as they clearly project well to topographically appropriate targets in ipsilateral motor cortex (Fig. 2M-P). Further, they make strong projections to ipsi- and contralateral entorhinal cortex (Fig. 2Q-X).

How accurately do these representative images convey the information contained in the whole dataset? To make quantitative comparisons, analysis proceeded as follows. Both the injection site location and the suprathreshold voxel intensity were used. For the injection sites, the distance between the center of mass of each injection was calculated as a distance offset (in millimeters, Fig. 3A). Because brains are aligned to standard coordinates, injection site offset is used as an estimate of the expected difference is in topographic location between two given injections. For axonal projections, all suprathreshold voxels for each injection are used. Pairs of injections are compared on a voxel-by-voxel basis using voxels that are suprathreshold for both injections. Voxels in ipsilateral and contralateral areas are compared based on regional identity in the Allen CCFv3, where each voxel is assigned to a specific brain region or cortical area. These areas include MOp and MOs for primary and secondary motor cortex as well as SSp-ul, SSp-bfd for the primary somatosensory cortex for upper limb and barrel field respectively. Depending on the analysis, cortical areas are pooled or analyzed by individual topographic areas. The Pearson Correlation Coefficient (PCC) is then computed based on voxel intensities (in arbitrary units, AU) in defined areas and used to assess the relationship for each pair of injections (Fig. 3B).

Example images of the ipsilateral cortex are shown for two aligned brains with somatosensory injections from anterior to posterior, spaced about 0.75 mm. Images range from frontal cortex (~1.75 mm anterior to bregma to ~1.25 mm posterior; Fig. 3C). Note the S1 axons in M1 (upper panels) and the brighter injection sites (lower panels). The injection site is always in left cortex, though differences in dominant paw might affect lateralization of function (Deemyad et al., 2022). Injections in S1 were generally stronger with brighter total voxel intensity when compared to M1 and frontal injections (Fig. 3E). However, the contralateral projections were relatively brighter in frontal injections based on the ratio of contralateral/ipsilateral intensity (Fig. 3F).

Injection sites in nearby locations in aligned brains showed high degrees of correlation in the targeting of their ipsilateral corticocortical projections (Fig. 3G). Examining the ipsilateral somatosensory plot (royal blue), injections with nearly no offset have greater than 0.6 correlation (linear fit near 0 offset). This drops quickly with even small offsets. Motor correlations (purple) follow a similar pattern, though the peak correlation is lower and the slope is not as steep. Frontal cortex (red) also shows a similar pattern to somatosensory, with very high (>0.7) nearby correlation, and very steep decline. Thus, ipsilateral corticocortical projections reliably target similar cortical areas across different animals. What about contralateral cortical projections? These also showed some correlation that varied with injection site offset (Fig. 3H).

But the pattern differed from ipsilateral cortex. Specifically, somatosensory cortex had correlations (light blue) that were lower than ipsilateral ones (Fig. 3I). Similarly, contralateral motor cortex projections (light purple) were not as well somatotopically organized as ipsilateral ones, though in general not as poor as those in somatosensory areas. Frontal cortex injections (pink) had quite strong corticocortical correlations for contralateral projections. The correlation data was also assessed in a similar manner for subdivisions of somatosensory, motor, and frontal cortex (vS1, fS1, orfS1, vM1, fM1, lIM1, M2, and ALM). However, because of the close proximity of injection sites within a single subdivision, linear fits assessing topographic precision were not as clear as with longer range injection pairs for comparison (Extended Data Fig. 3).

In addition to making these comparisons across different injection cases, comparing each brain to the contralateral side allowed a direct assessment of symmetry. Correlations were computed for each injection site by comparing ipsilateral cortex to the aligned and reflected contralateral corticocortical projections (Fig. 4A). Example injections in aligned brains are shown for somatosensory, motor, and frontal (Fig. 4C-E) injections. As before, these sections of aligned brains are shown from anterior (top) to posterior (bottom). There is a remarkable difference in symmetry across the dorsal cortex. Frontal cortex injections have PCC ~0.45, while motor areas are slightly <0.30 and somatosensory ones are ~0.10 (Fig. 4B). This is

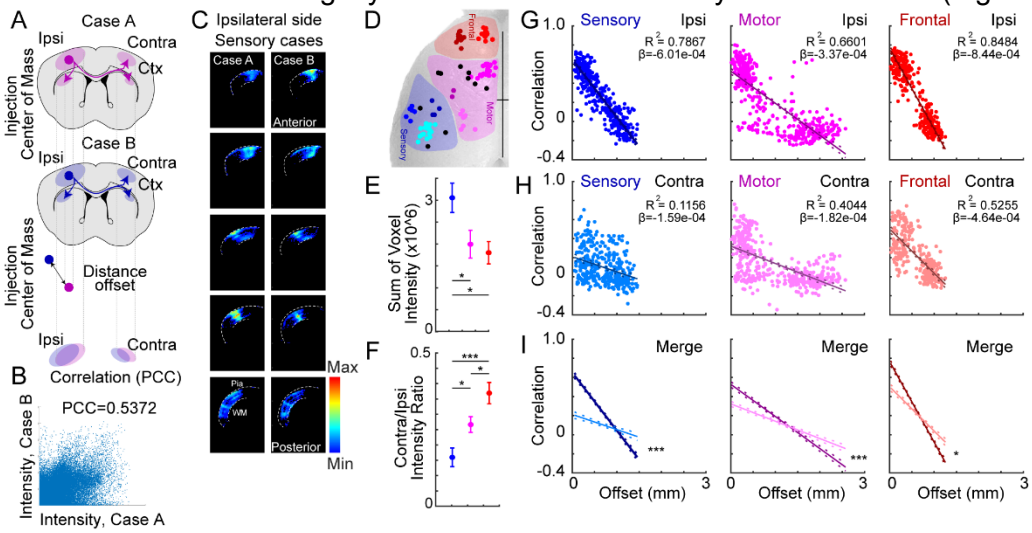

Figure 3 | Topographic organization of contralateral cortical projections in frontal, motor, and somatosensory cortex
(A) Schematic illustrating how the corticocortical projections from two different injection sites are compared. The center of mass of cell bodies at the injection site is compared (offset distance in mm). The overlap of the ipsilateral of contralateral projections can be compared. (B) The correlation coefficient (PCC) for two example cases, comparing the suprathreshold voxel intensities for ipsilateral cortical projections. PCC=0.5372 for this example. (C) Sample coronal planes from two cases of aligned brains showing only suprathreshold ipsilateral cortical voxels. Spacing is ~0.75 mm along the anterior/posterior axis, from ~1.75 mm anterior to ~1.25 mm posterior. (D) Injection site locations in sensory, motor, and frontal locations. (E) Measurement of the total voxel intensity for ipsilateral cortical projections. Voxels range from 0-255 (in arbitrary units). Sensory injections were brighter than motor and frontal. Mean with SEM. 1 way ANOVA; df=2, F=4.89, p=0.00997. Tukey-corrected pairwise t-tests: Frontal–M1 (p=0.893), S1–M1 (p=0.035), S1–Frontal (p=0.015). (F) Ratio of voxel intensity for ipsilateral (injection site side) and contralateral voxels. 1 way ANOVA; df=2, F=12.07, p=2.66e-5. Tukey-corrected pairwise t-tests: Frontal–M1 (p=0.04), S1–M1 (p = 0.028), S1–Frontal (p = 0.000014). (G) Comparison of ipsilateral cortical correlations between injection sites for sensory, motor, and frontal injections. Mean with SEM. (H) Comparison of contralateral cortical correlations between injection sites for sensory, motor, and frontal injections. (I) Linear regression with 95% confidence interval. Two way ANCOVA examined the effects of region and ipsi/contra location on correlation (PCC) after controlling for distance (F(2,2165)=16.1, p=1.14e-7). Pairwise comparisons were computed and Bonferroni adjusted and all regions had significantly higher slopes for ipsi versus contra: S1 (F(2165)=9.87, adj. p=1.63e-22), M1 (F(1,867) = 13.8, p=2.12e-4), and Frontal (F(2165)=2.33, adj. p=2.01e-2).

consistent with substantially greater symmetry in corticocortical innervation in anterior (as opposed to posterior) corticocortical projections.

Symmetry was further assessed as follows. First, it is clear that corticocortical projections in a defined cortical region do not simply target the corresponding cortical area in the contralateral side of the brain, but also project to a range of ipsilateral and contralateral targets (Szczupak et al., 2023). For contralateral corticocortical output, homotypic projections are those that target the corresponding region of cortex in the other hemisphere. Heterotopic projections target other cortical areas, often adjacent ones (Fig. 4F). Using the CCFv3 regions to define these borders, heterotopic axonal projections were indeed stronger to heterotopic than to

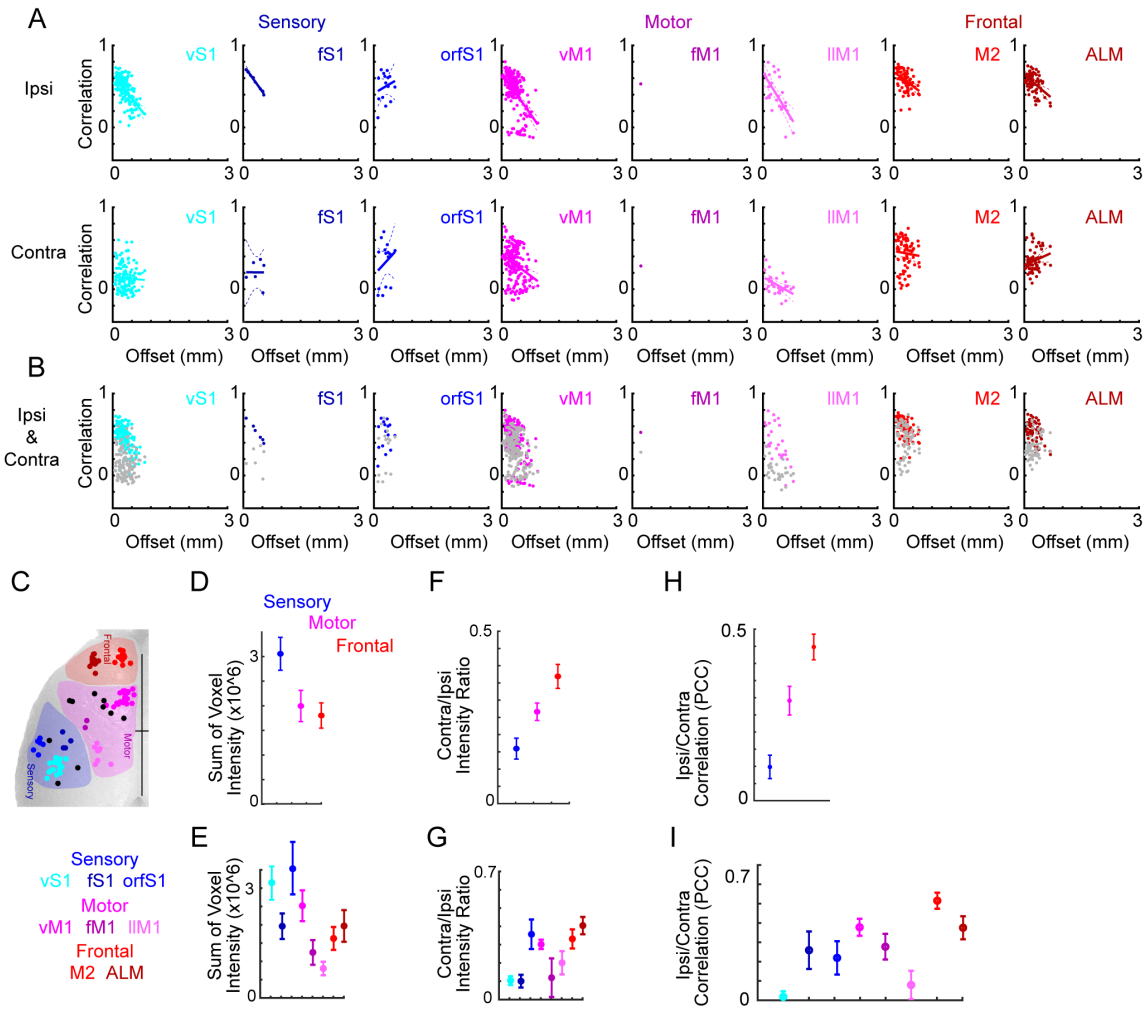

Extended Data Figure 3 | Topographic organization of contralateral cortical projections in frontal, motor, and somatosensory cortex (A) Comparison of ipsilateral (top row) and contralateral (bottom row) cortical correlations between injection sites for sensory, motor, and frontal injections. Subgroups within areas presented in different colors. Linear fit and 95% confidence interval (dotted line) plotted. (B) Comparison of ipsilateral (colors) and contralateral (gray) cortical correlations between injection sites for sensory, motor, and frontal injections. (C) Schematic of injection site locations. (D,E) Sum of ipsilateral voxel intensity by injection site location, with subdivision of cortical sites into finer divisions at bottom. (F,G) Ratio of contralateral to ipsilateral voxel intensity, with subdivision of cortical sites into finer divisions at bottom. (H,I) Overall correlation between ipsilateral and contralateral voxels by injection site, with subdivision of cortical sites into finer divisions at bottom.

homotopic targets (Fig. 4G-H), with heterotopic projections comprising 70-90% of contralateral projections. However, because the CCFv3 contained several somatotopic subdivisions for somatosensory cortex, it was possible to assess the degree to which heterotopic axons targeted the same distribution of cortical areas in each hemisphere. Total axonal projection intensity to each CCFv3 cortical area (summed across layers) was computed and plotted across all cortical regions (Fig. 4I for somatosensory cortex injections). Ipsilateral intensity (solid line) was generally higher than contralateral intensity (dotted line). Most projections were in somatomotor areas, so these were expanded in detail for sensory (blue), motor (purple), and frontal (red; Fig. 4J). Because contralateral intensity was generally lower, normalized distributions of ipsi- and contralateral intensity were plotted to compare the pattern (Fig. 4K), with generally similar results across all areas. Because of the somatosensory subdivisions within CCFv3, it was also possible to individually assess vS1 (SSp-bfd), fS1 (SSp-ul), and orfS1 (SSp-n) in the same manner (Fig. 5I-L). These largely showed different distributions between different areas (vS1 versus fS1) but similar patterns between ipsi-lateral and contralateral projections (Fig. 5K).

Because of the alignment to a standard atlas, symmetry was also assessed by reflecting the projections from the contralateral side and subtracting them from the ipsilateral side. Because the structures are 3D, they are presented in figures as a projection (summing along the dorsoventral axis). For cortex, this results in a map that appears as a view from the dorsal surface (Fig. 5A-H). Injection site intensity (marked with red circles) is reflected in yellow with high ipsilateral intensity. Cortical areas unrelated to somatomotor injection sites are close to background (appearing black). These maps helped identify areas with substantial ipsilateral projections, such as connections between M1 and S1, as well as projections to entorhinal cortex. In S1 injections, corticocortical projections target secondary somatosensory cortex (S2) as well as entorhinal areas in both ipsi- and contralateral hemispheres. Remarkably,

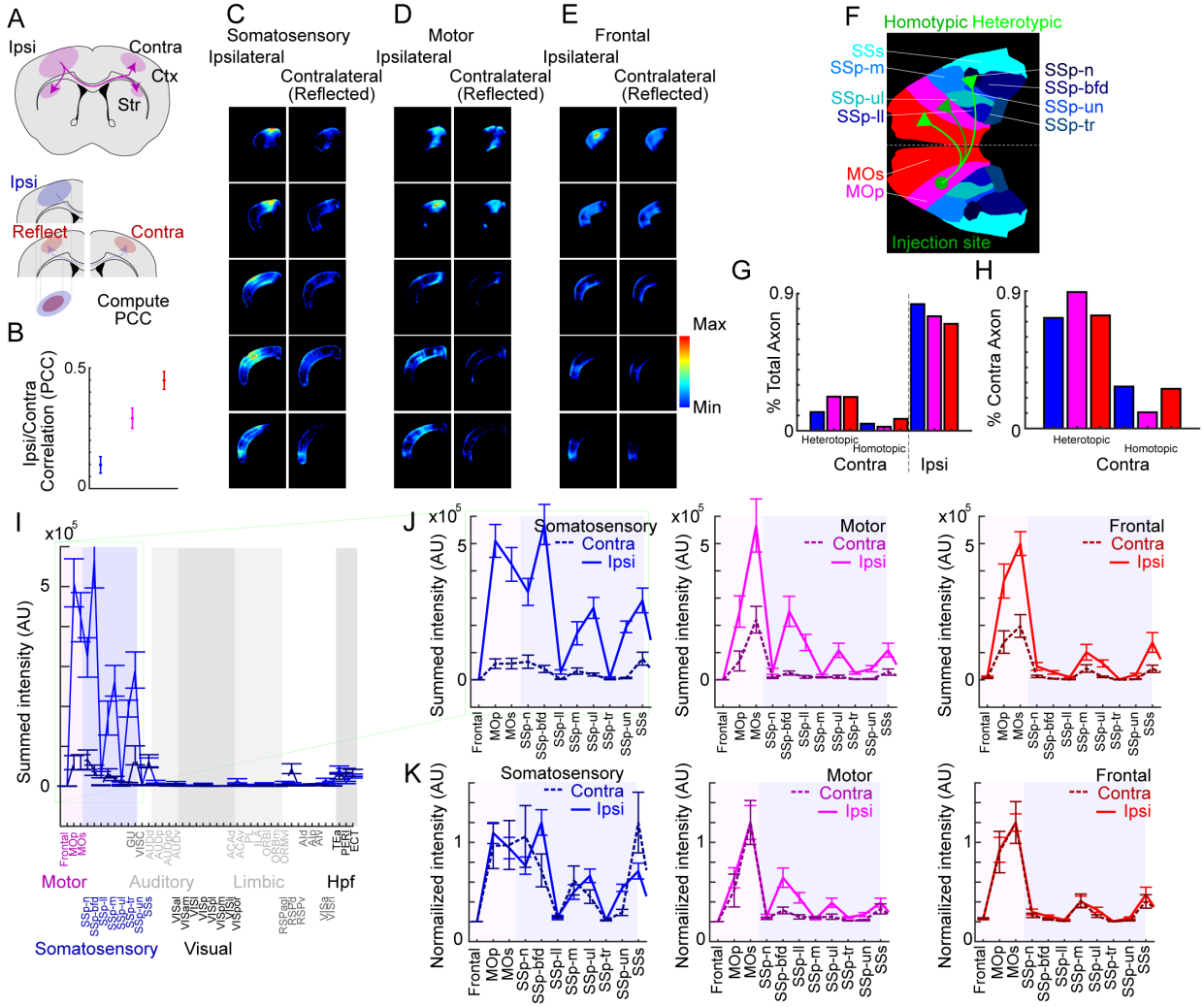

Figure 4 | Area-by-area comparison of ipsi- and contralateral corticocortical projections in frontal, motor, and somatosensory cortex
(A) Schematic comparing corticocortical projections from a single injection site between ipsilateral and contralateral targets. (B) Average overall correlation (mean with SEM). (C-E). Sample coronal planes from aligned brains for somatosensory (C), motor (D), and frontal (E) injections. Left columns show ipsilateral cortex (injection side). Right columns show contralateral cortex, reflected for comparison. Only suprathreshold cortical voxels are shown. Spacing is ~0.75 mm along the anterior/posterior axis, from +1.75 mm anterior to -1.25 mm posterior. (F) Topographic areas of cortex in the Allen CCFv3. To compare contralateral cortical projections, homotypic projections are contralateral projections from one cortical area (the injection site) to the corresponding cortical area (dark green), while heterotopic projections (light green) target contralateral cortex in areas not corresponding to the injection site. (G-H) Quantification of the fraction of contralateral corticocortical projections to ipsi- and contralateral areas based on suprathreshold voxel intensity. All somatosensory (blue), motor (purple), and frontal (red) injections are combined. (I-K) Projection intensity to somatomotor cortical areas (per CCFv3) from somatosensory (blue), motor (purple), and frontal (red) injections. Regions are summed across cortical layers, noted on the x-axis in CCF nomenclature. All areas are displayed for somatosensory cortex injections (I), with only somatomotor areas (J-K) displayed at right (where most axons are present). The summed intensity (in arbitrary units, AU) for suprathreshold voxels is plotted in (I) and (J). Solid lines are for ipsilateral projections and dotted lines are for contralateral injections. (K) represents peak normalized plots of the ipsilateral (solid) and contralateral (dotted) projection intensity. Ipsi- and contralateral intensity each normalized separately to compare the ipsi- and contralateral patterns in an intensity-independent manner.

contralateral entorhinal cortex received stronger projections from orfS1(white dotted line and red arrow in Fig. 5C) (Mao *et al.*, 2011). Motor areas send projections to principally ipsilateral somatosensory cortex, though this is most apparent in vM1 injections (green arrow, Fig. 5D), as whisker areas in M1 and S1 are sufficiently separate to distinguish projections, which forelimb areas are adjacent, which obscures this. These areas also project to entorhinal areas (white arrows, Fig. 5E-F). Frontal areas also have strong connectivity with ipsilateral motor areas (white arrows, Fig. 5G-H).

High correlation of projection targeting in corticostriatal projections

Similar patterns were present in a subset of corticostriatal projections examined (Fig. 6). Corticostriatal projections target topographically defined regions of striatum(Foster et al., 2021; Hintiryan *et al.*, 2016; Hooks *et al.*, 2018). Thus, frontal cortex densely targets ipsi- and contralateral striatum (Fig. 6A-C), while motor (Fig. 6D-F) and somatosensory (Fig. 6G-I) cortices target dorsolateral striatum. To compare the ipsi- and contralateral projections to striatum (Fig. 6L-N) at different rostrocaudal planes, images from injection sites in frontal cortex (Fig. J-K) are shown, with detail in the striatum at three rostrocaudal planes (Fig. 6O-T).

Injections were quantitatively compared as before. The distance offset was calculated in millimeters, while the correlation coefficient of overlapping suprathreshold voxels was computed for pairs of injections (Fig. 7A-B). Striatal voxel identity was determined by registration to the Allen CCFv3. Example images of the contralateral striatum are shown for two aligned brains for a frontal injection site, with planes spaced at 0.75 mm ranging from ~1.50 mm anterior to bregma to ~1.50 mm posterior (Fig. 7C). Striatal projections were strongest from frontal areas in mouse (Fig. 7E), with summed voxel intensity more than twice that of motor and somatosensory injections. Furthermore, projections to contralateral striatum were also relatively brighter in frontal injections based on the ratio of contralateral/ipsilateral intensity (Fig. 7F). This effect was more strongly pronounced in striatum than in cortex.

As for cortical injections, injection sites in nearby locations in aligned brains showed high degrees of correlation in the targeting of their ipsilateral striatal projections (Fig. 7G), which has previously been examined in detail(Hooks *et al.*, 2018). Adding to this prior study of motor and sensory corticostriatal topography, the frontal injections also show high topographic organization, with the ipsilateral corticostriatal projections of frontal cortex (red) being perhaps more precise than somatosensory ones. Peak PCC with no offset is ~0.7 (linear fit near 0 offset). In comparison, peak somatosensory PCC (royal blue) is ~0.6 and motor (purple) is ~0.4. Thus, ipsilateral corticostriatal axons also reliably target to similar cortical areas across different animals. Contralateral striatal projections also showed an unexpected pattern. As in cortex, these showed correlation that varied with injection site offset (Fig. 7H). But somatosensory cortex, which had remarkably high correlation in ipsilateral connectivity, had relatively poor correlations (light blue) on the contralateral side (Fig. 7H). Further, contralateral motor cortex projections to striatum (light purple) were not as well organized as ipsilateral projections. As in cortex, there were not as weak as somatosensory ones. But contralateral corticostriatal projections from frontal cortex (pink) were remarkably similar. The fit was difficult to distinguish between ipsi- and contralateral projections (Fig. 7I).

This suggested a high degree of symmetry in the strong corticostriatal projections. Thus, the contra- and ipsilateral side of each brain were compared by reflecting the registered contralateral projections (Fig. 7C-D). Examples are shown for both motor (Fig. 7C) and frontal cases (Fig. 7D), with frontal projections having much stronger connectivity to ventral striatum. Symmetry was impressive for frontal projections, with the average PCC ~0.6 for frontal cortex. In marked contrast, this symmetry was largely absent in motor and somatosensory cases, with PCC ~0.2 for both. Having established that there was a rostrocaudal gradient in the symmetry of corticostriatal projections, it was of interest to test for a medial-lateral gradient. The frontal cortex injections used could readily be sorted into more medial (M2) or lateral (ALM)

locations(Hooks *et al.*, 2018) (note the names for these regions vary; see Discussion). Comparing these did not reveal substantial differences in the degree of symmetry between frontal injection sites (Extended Data Fig. 7I, t-test, p=0.064). Overall, this data suggests that corticostriatal projections can show even greater symmetry than corticocortical projections, and that this symmetry varies principally along the rostrocaudal axis, with symmetry highest in frontal areas. Note that this was not tested in posterior parietal areas or other sensory areas such as auditory and visual cortex.

Taking advantage of the alignment to a standard atlas, symmetry was similarly assessed by reflecting the projections from the contralateral striatum and subtracting from the ipsilateral striatum. Striatal voxels are then presented as a dorsoventral projection, summed along the

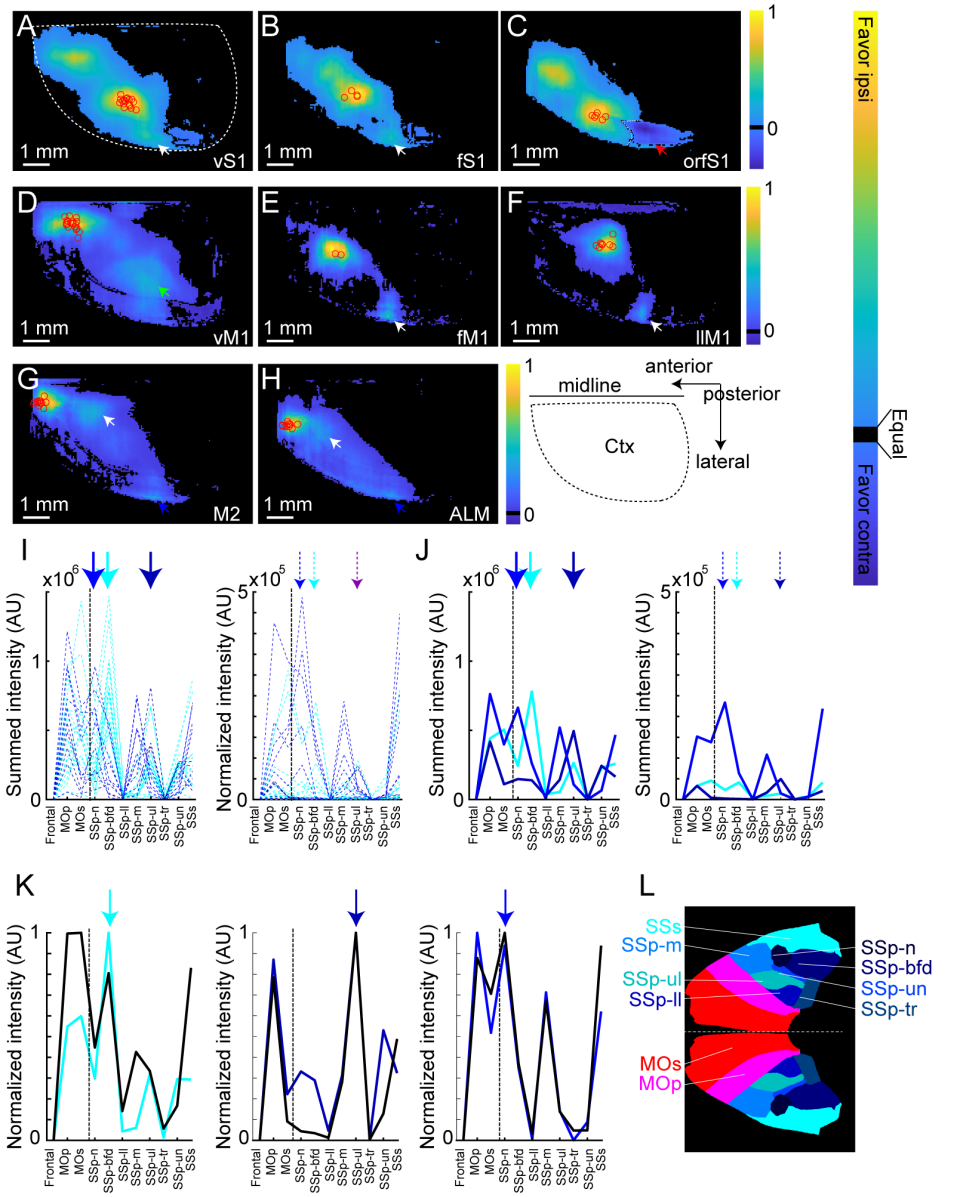

Figure 5 | Symmetry of corticocortical projections in frontal, motor, and somatosensory cortex
(A-H) Injection sites in somatosensory (A-C), motor (D-F), and frontal (G-H) cortex, subdivided into topographic subregions (vS1, fS1, and orfS1 for somatosensory, A-C; vM1, fM1, lIM1 for motor, D-F; and M2 and ALM for frontal, G-H). Injection sites are marked by red circles. Heatmap represents normalized projection intensity in ipsilateral cortex (summed across the dorsoventral axis), with contralateral intensity subtracted. Relative intensity is shown in the color map (yellow, stronger on the ipsilateral side; dark blue, stronger on the contralateral side). The outline of the dorsal surface of cortex is shown in (A). Black pixels represent values close to zero (contralateral and ipsilateral intensity roughly equal). (A-C) White arrowheads indicate strong ipsilateral connectivity with secondary somatosensory cortex (SSs). Red arrowheads indicate strong contralateral connectivity with entorhinal cortex. (D-F) Green arrowheads indicate strong motor projections to ipsilateral somatosensory cortex (SSp-bfd). White arrowheads indicate strong ipsilateral connectivity with secondary somatosensory cortex (SSs).
(G-H) White arrowheads indicate strong ipsilateral connectivity with primary motor cortex (MOp). (I-K) Projection intensity to all cortical areas (per CCFv3) from subregions of somatosensory cortex injections. Left plot (I and J) shows the summed intensity (in arbitrary units, AU) for suprathreshold voxels in ipsilateral cortex for each individual case (color coded to the subregion), with arrow at top indicating the CCFv3 region best corresponding to the injection site. The right plot shows the same data for the contralateral side. The mean of the ipsilateral (left) and contralateral (right) is presented in (J). Normalized plots of ipsilateral (blue colors) and contralateral (black) are presented in (K) for vS1 (left), fS1 (middle), and orfS1 (right). (L) Color coded plot of the CCFv3 areas for somatosensory cortex.

479 dorsoventral axis (Fig. 8A-H). For striatum, this results in a paisley-shaped map viewed from
480 above. High projection site intensity is reflected in yellow for high ipsilateral intensity. Unrelated
481 striatal areas are close to background (black). These maps were largely consistent with the
482 topographic targeting of somatosensory and frontal corticostriatal projections previously
483 described, with slight differences between cortical injection site subdivisions (Fig. 8A-F).
484 However, this map also identified areas in the anterolateral striatum (arrowheads and dotted
485 lines) where contralateral corticostriatal projections were more intense than ipsilateral ones (Fig.
486 8D,G,H). This might be one small specialization in the contralateral corticostriatal projection.
487 Overall, these results suggest largely symmetrical corticostriatal projections in frontal areas,
488 which are also stronger than those in motor or somatosensory cortex.
489
490 **Discussion**
491
492 **Differences in function, somatotopy, and symmetry of cortical areas**
493 Inferring function from anatomy is a challenge because the influence given connections
494 have between different brain areas could vary considerably when cell types are targeted in
495 different ways. Furthermore, for cortical circuits especially, how information is encoded is not yet
496 clear for many features, especially higher order features such as motor planning and decision-
497 making. The projection tracing here considers three major aspects of neocortex spread over
498 dorsal cortical areas anterior to visual cortex. Primary somatosensory cortex is thought to
499 encode incoming touch information, organized in a somatotopic manner. This somatotopy is
500 quite precise, visually encapsulated by thalamic afferents from VPM which target a single
501 whisker barrel in layer 4. Although different cells might extract specific features of sensory
502 experience, such as touch direction, information is integrated across a broader area outside of
503 cortical layer 4. To the extent that primary somatosensory cortex exists to provide a faithful
504 representation of salient features of current sensory perception of the contralateral body, the
505 role for contralateral somatosensory information is diminished. Callosal corticocortical afferents
506 are visibly present, however, targeting the local cortical circuit in a similar laminar pattern in both
507 ipsilateral and contralateral cortex(Petreanu *et al.*, 2007). Consistent with this, relatively weak
508 corticocortical and corticostriatal projections exist based on the intensity of axonal fluorescence
509 (Fig. 3 and 6). These afferents are capable of plasticity during sensory manipulation, such as by
510 whisker elimination(Petrus et al., 2020; Petrus et al., 2019). This advances the hypothesis that
511 such connections, though weak, may exist to expand in cases where plasticity may be adaptive,
512 such as following lesions. One testable hypothesis might be that, in addition to callosal
513 projections compensating for lesions in a cerebral hemisphere, that regions with stronger
514 callosal projections might have plasticity that results in more rapid or effective expansion to take
515 over features of the lesioned side. These projections are generally consistent with segregated
516 cortico-basal ganglia-thalamic loops for performing computations on incoming sensory
517 information.
518 Primary motor cortex supports a different function than primary somatosensory cortex.
519 Although these are adjacent and both contain a similar somatotopic map, the somatotopy
520 differs. Ascending sensory information targets the cortex with great precision, as exemplified by
521 barrels representing single whiskers in mice (which anatomically correspond to the highly
522 restricted axonal arborizations of primary thalamic relay neurons). In contrast, motor cortex
523 potentially has less precision. Microstimulation maps have imprecisely defined borders, in part
524 because they vary with the current used to evoke movement(Brecht *et al.*, 2004; Hooks *et al.*,
525 2011; Li and Waters, 1991; Tennant *et al.*, 2011). These also vary considerably between
526 animals(Tennant *et al.*, 2011). This change in somatotopy between S1 and M1 is reflected in the
527 more rapid decrease in correlation of striatal targeting for injections placed a small distance
528 apart in sensory versus motor cortex{(Hooks *et al.*, 2018). Remarkably, the precise somatotopy
529 of ipsilateral projections is largely reduced in contralateral cortex and striatum. But some of it is

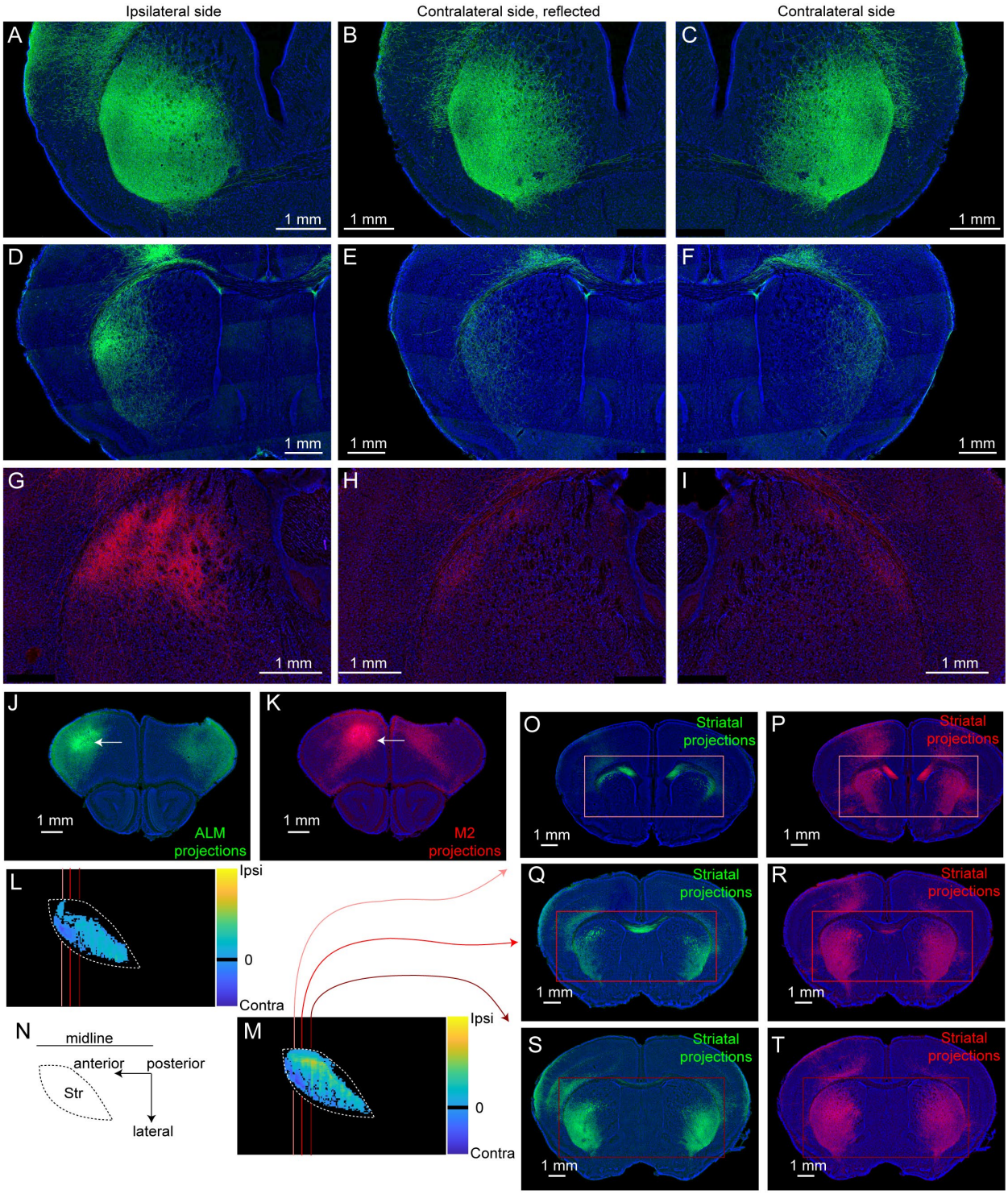

Figure 6 | Ipsi- and contralateral corticostriatal projections of IT-type neurons in frontal, motor, and somatosensory cortex
(A-I) Coronal images showing injection site of AAV-DIO-XFP into frontal cortex (A-C), motor cotex (D-F), and somatosensory cortex (G-I). Left column shows ipsilateral side, right column shows contralateral side, with reflected image shown for comparison. (J-T) More detailed presentation of the injection sites in ALM (J, green) and M2 (K, red) and their striatal targets. Arrowheads show axonal projections. (L-N) present the overall difference in striatal axonal intensity between ipsilateral and contralateral projections (see Fig. 8) for the ALM (L) and M2 (M) injections, with a schematic of the dorsal view of striatum (Str). Red lines indicate approximate planes of the images in (O-T), with the striatum boxed in the corresponding color.

retained in motor cortex (Fig 4B), though it is equally poor in contralateral striatum (Fig. 7B). What might the function of callosal projections be in motor areas? While many motor features

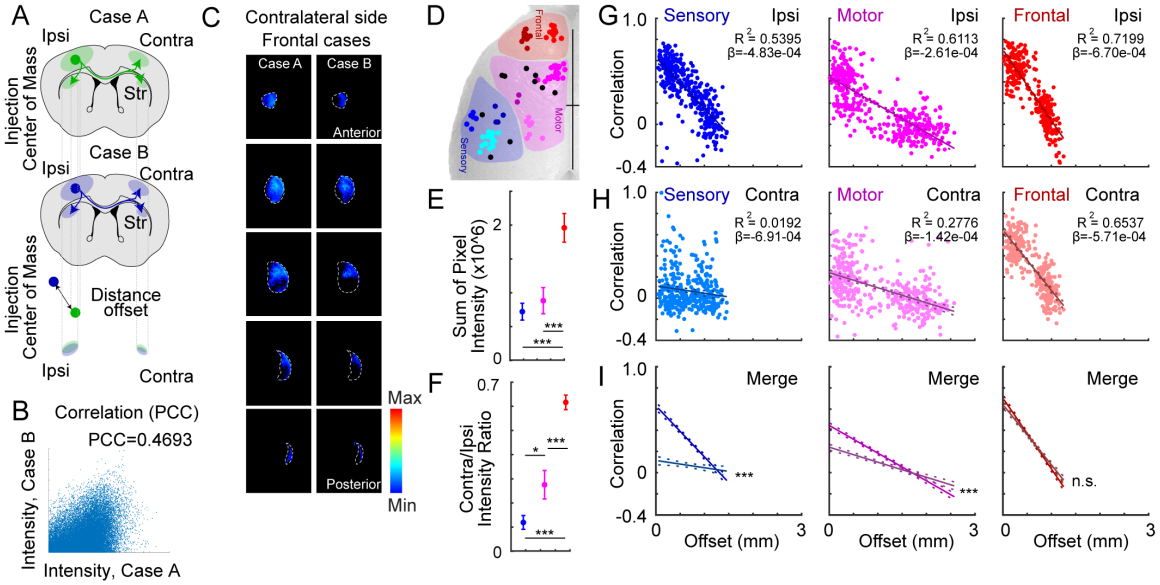

Figure 7 | Topographic organization of contralateral corticostriatal projections in frontal, motor, and somatosensory cortex
(A) Schematic illustrating how the corticostriatal projections from two different injection sites are compared. The center of mass of cell bodies at the injection site is compared (offset distance in mm). The overlap of the ipsilateral of contralateral projections can be compared. (B) The correlation coefficient (PCC) for two example cases, comparing the suprathreshold voxel intensities for ipsilateral striatal projections. PCC=0.4693 for this frontal example. (C) Sample coronal planes from two cases of aligned brains showing only suprathreshold contralateral striatal voxels. Spacing is ~0.75 mm along the anterior/posterior axis, from ~1.50 mm anterior to ~1.50 mm posterior. (D) Injection site locations in sensory, motor, and frontal locations. (E) Measurement of the total voxel intensity for ipsilateral striatal projections. Voxels range from 0-255 (in arbitrary units). Frontal injections were brighter than somatosensory and motor. Mean with SEM. 1 way ANOVA; df=2, F=13.63, p=8.21e-6. Tukey-corrected pairwise t-tests: Frontal–M1 (p=1.5e-4), S1–M1 (p=0.787), S1–Frontal (p=2.1e-5). (F) Ratio of voxel intensity for ipsilateral (injection site side) and contralateral voxels. 1 way ANOVA; df=2, F=32.84, p=4.18e-11. Tukey-corrected pairwise t-tests: Frontal–M1 (p=1.0e-6), S1–M1 (p=0.03), S1–Frontal (p<1e-16). (G) Comparison of ipsilateral striatal correlations between injection sites for sensory, motor, and frontal injections. (H) Comparison of contralateral striatal correlations between injection sites for sensory, motor, and frontal injections. (I) Linear regression with 95% confidence interval. Two way ANCOVA examined the effects of region and ipsi/contra location on correlation (PCC) after controlling for distance (F(2,2165)= 67,565, p=3.45e-29). Pairwise comparisons were computed and Bonferroni adjusted and all regions had significantly higher slopes for ipsi versus contra: S1 (F(2162)=16.7, adj. p=3.46e-59), M1 (F(2162)=6.46, adj. p=1.3e-10), and Frontal (F(2162)=2.33, adj. p=0.91).

move one limb or body part independently, some features require coordination, either due to the manipulation of a single object with two hands, or to coordinate movement of the lower limbs for balance (a function for which spinal circuits also exist). Consistent with this, the crossed corticostriatal input is stronger in leg and trunk regions than for hands(Borra *et al.*, 2022).

The topographic organization of frontal projections was unexpected, as this area is not previously mapped with the same precision as sensory and motor areas. The anterior dorsal surface of mouse cortex, is subdivided and assigned different names including also called secondary motor (MOs(Wang *et al.*, 2020; Zingg *et al.*, 2014)) or M2(Hooks *et al.*, 2013)), anterior lateral motor (ALM(Komiyama *et al.*, 2010)), lateral and medial agranular (AGl and AGm(Li and Waters, 1991)) and FrA(Paxinos and Franklin, 2004). That is may be somatotopically organized is suggested by the corticocortical connectivity with other somatotopically defined regions of primary motor and somatosensory cortex(Zingg *et al.*, 2014). It is not clear from microstimulation studies that a complete, well-resolved body representation exists in frontal cortex, though a rostral forelimb domain is suggested(Tennant *et al.*, 2011). Our data here show that projections from frontal cortex to cortical and striatal targets are well-organized and reliably project to appropriate targets in the ipsi- and contralateral hemispheres. Projection patterns in ipsilateral cortex (Fig. 3G) and ipsilateral striatum (Fig. 6G) are as sensitive to small displacements as in somatosensory areas. Furthermore, this topographic precision is maintained in the contralateral projection (Fig. 3H and Fig. 6H), making frontal cortex connectivity highly symmetric (Fig. 7B). There did not seem to be a large difference in symmetry of the contralateral projection between medial and lateral sites (ALM versus M2; Fig.

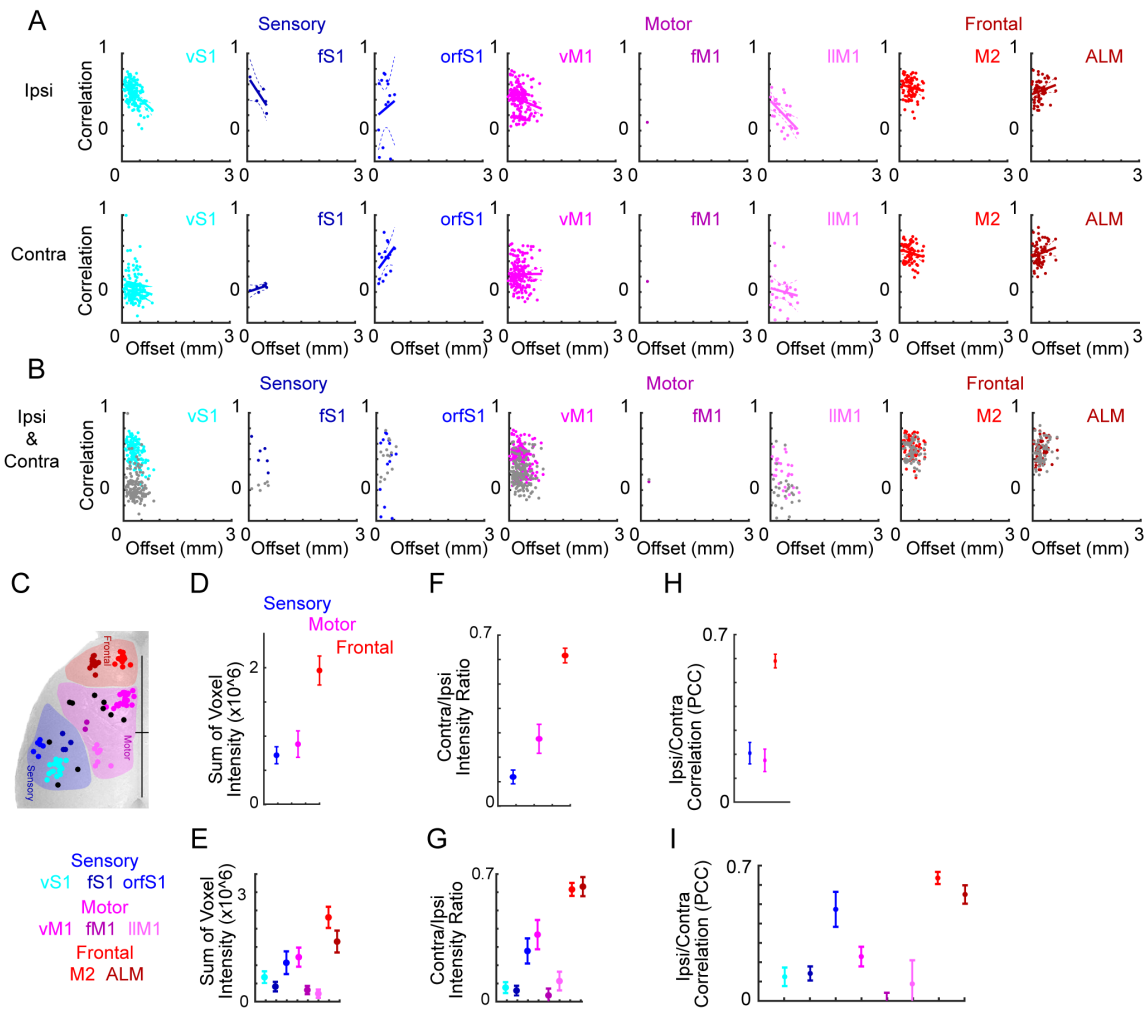

Extended Data Figure 7 | Topographic organization of ipsi- and contralateral corticostriatal projections
(A) Comparison of ipsilateral (top row) and contralateral (bottom row) corticostriatal correlations between injection sites for sensory, motor, and frontal injections. Subgroups within areas presented in different colors. Linear fit and 95% confidence interval (dotted line) plotted. (B) Comparison of ipsilateral (colors) and contralateral (gray) corticostriatal correlations between injection sites for sensory, motor, and frontal injections. (C) Schematic of injection site locations. (D,E) Sum of ipsilateral voxel intensity by injection site location, with subdivision into finer divisions by injection site at bottom. (F,G) Ratio of contralateral to ipsilateral voxel intensity, with subdivision into finer divisions by injection site at bottom. (H,I) Overall correlation between ipsilateral and contralateral voxels by injection site, with subdivision into finer divisions by injection site at bottom.

7B), suggesting the gradient of topographic precision in the contralateral projections varies mostly along the anterior-posterior axis.

Although this investigation did not span to other cortical areas, it would be of interest to understand whether the organization of other cortical regions follows similar rules. For example, visual cortex might be expected to be similar to somatosensory cortex, in that each hemisphere would have weaker callosal connectivity, as the principal function is to represent visual stimuli in the contralateral visual field. Weak contralateral connectivity would be consistent with the rostrocaudal gradient seen here. Auditory cortex is positioned posteriorly and represent acoustic stimuli. But, as incoming acoustic information from a single location might reach both ears, perhaps there would be more value for an interhemispheric connection than for visual or touch stimuli. Further, some higher order areas in parietal cortex that represent more abstract concepts might be interesting to evaluate similarly.

Organization and strength of the corticostriatal projection

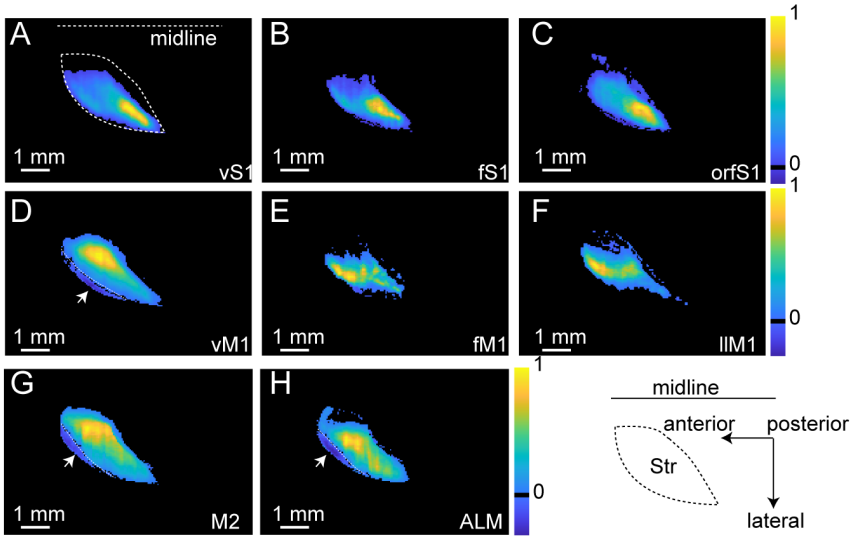

Figure 8 | Symmetry of corticostriatal projections from frontal, motor, and somato-sensory cortex
(A-H) Striatal projections from injection sites in somatosensory (A-C), motor (D-F), and frontal (G-H) cortex, subdivided into topographic subregions (vS1, fS1, and orfS1 for somatosensory, A-C; vM1, fM1, lIM1 for motor, D-F; and M2 and ALM for frontal, G-H). Injection sites are not marked. Heatmap represents normalized projection intensity in ipsilateral striatum (summed across the dorsoventral axis), with contralateral intensity subtracted. Black pixels represent values close to zero (contralateral and ipsilateral intensity roughly equal), with yellow representing sites with stronger ipsilateral strength (injection sites) and dark blue voxels representing stronger contralateral sites. White arrowheads reflect anterolateral sites of strong contralateral connectivity. Schematic inset at bottom right shows the shape of striatum as viewed from the dorsal side, with midline and anterior/posterior axis labeled.

New methods to target specific cellular components result in a more detailed understanding of the organization of basal ganglia circuitry. The main features are the convergence of excitatory cortical (and some thalamic) input from a large number of afferents onto the spinal projection neurons in striatum, which in turn project either in the indirect pathway (to external globus pallidus) or the direct pathway (to substantia nigra pars reticulata and internal globus pallidus/entopeduncular nucleus), with some convergence onto a smaller number of neurons at each step, eventually outputting to thalamus and brainstem(Lee *et al.*, 2020). This data then tests the concept that cortical output generally forms loops from cortex through basal ganglia and thalamus that are largely parallel and functionally segregated(Alexander *et al.*, 1986).

These data quantify the substantial contralateral corticocortical and corticostriatal projections. In striatum, the contralateral striatal projection from frontal areas was ~65% the strength of the ipsilateral projection (Fig. 6E-F). This was considerably weaker for M1 (~25%) and S1 (~15%). Similarly, cortex has a similarly pattern of contralateral cortical projections, though the values were somewhat closer (Frontal, ~37%; M1, ~27%; S1, ~17%). Crossed projections are also believed to be stronger from frontal and cingulate areas than from S1 in non-human primates as well(Borra *et al.*, 2022). Further, the data suggest that the crossed corticocortical connection instead of the direct corticostriatal one is more effective in causing sensory responses to ipsilateral touch(Reig and Silberberg, 2016). Anatomical data in other species is consistent with these results. Retrograde tracer injections in striatum label frontal cortex relatively symmetrically while barely labeling the contralateral parietal cortex(Borra *et al.*, 2022). Notably, primate posterior parietal cortex (Area 7) does indeed also project contralaterally to topographically similar striatal targets as ipsilateral afferents, though less extensively(Cavada and Goldman-Rakic, 1991). Along the rostro-caudal gradient of the striatum, sectors closer to the caudate head are more likely to receive converging input from

ipsi- and contralateral cortex, while the tail may receive almost exclusively ipsilateral input (Griggs et al., 2017). Although a simplified interpretation of the data suggests a rostal-caudal gradient in contralateral connectivity, midline crossing projections from more associative cortex (such as frontal as well as posterior parietal) suggests a functional gradient: regions involved in direct sensory processing may be less likely to have midline crossing projections, while cortical areas related to more executive functions, such as categorization, sensory-motor coordination, and decision-making, are more likely to have stronger contralateral connectivity to allow brain areas to integrate information and act as a single unit. However, data from rats (Alloway *et al.*, 2006) suggests a reasonably strong contralateral cortical projection based on retrograde tracing from striatum.

Convergence of ipsilateral and contralateral projections in the striatum

These data reveal a relatively strong and remarkably symmetric organization of the frontal output to striatum. First, both medial and lateral frontal areas (M2 and ALM in the terminology of (Hooks *et al.*, 2018)) show remarkably strong correlation in their projections to ipsilateral and contralateral cortex and striatum. Small displacement in the injection site cause shifts in the targeting of projections when compared across animals (Fig. 3G-I and Fig. 6G-I). That these correlations are as precise as somatosensory cortex suggests the possibility of some kind of topographic representation in frontal areas, though the degree to which this is motor-related or decision-related is unclear. Little is known about differences in cellular targeting of such projections. Whether these connections target direct or indirect pathway striatal projection neurons (Wall et al., 2013), which suggested M1 favored indirect pathway targets, while S1 favored direct pathway targets using retrograde tracing approaches. Whether this targeting differs for ipsi- and contralateral targets (Johansson and Silberberg, 2020) was also tested for M1 using physiological means, but differences for direct and indirect pathway connectivity were not pronounced. Similar tests have not been performed for frontal projections.

What is the purpose of such effective convergence from homotopic areas in cortex and striatum? It makes sense that sensory information is largely segregated because of the cortex representing information from the contralateral side of the body or the visual field; the weaker crossed projections limit the influence of contralateral information on faithful reporting of current sensory information. Likewise, though there is some need for the motor system to coordinate movement across the midline, such as guiding the forelimbs to grasp an object, it also is understandable that at times the limbs move independently (reflected in differences, perhaps in the strength of crossed projections for different regions in the motor somatotopic map more readily measured in primates).

For frontal areas and their role in executive function, these areas seem more arranged to provide input to each other and converge on a single decision for the animal. Indeed, the motor plan can be stored in one side of frontal cortex during blockade or silencing (and restored to the other side following relief), suggesting that these indeed do operate in concert (Guo et al., 2014; Li et al., 2016). Thus, the purpose of well-organized, near symmetrical projections from frontal areas may be to allow a unitary sense of decision-making and executive function to emerge from the circuit, and to use the striatal projections to perform the same computation on incoming information in parallel, potentially supporting robust decision-making.

Figure Legends:

Figure 1 | Mapping layer 5 corticostriatal output from sensory and motor cortex
Injection site of AAV-DIO-XFP into frontal (A), motor (B), and sensory cortex (C) of Tlx3_PL56-Cre+ mice. Inset of coronal brain slices shows approximate location. In (A), top-down cartoon shows approximate planes of section. (D) Center of mass of all injection sites in sensory (blue, N=27), motor (purple, N=30), and frontal (red, N=25) cortex. Subdivisions within areas (M2, ALM, vM1, fM1, lIM1, vS1, fS1, and orfS1) are indicated in different colors, with uncategorized injection sites in black. Bregma is indicated as the cross at top right. (E) Quantification of relative depth of labeled Cre+ cortical neurons in frontal (red), motor (purple), and sensory (blue) cortex. (F) Cartoon of output targets of IT-type neurons.

Figure 2 | Ipsi- and contralateral projections of IT-type neurons in frontal, motor, and somatosensory cortex
(A-D) Coronal images showing injection site of AAV-DIO-XFP into frontal cortex (ALM), with ipsi- (B) and contralateral (D) cortex presented for comparison. Reflected image of contralateral side (C) shown for comparison. (E-H) Similar presentation for motor cortex (fM1) injection. (I-L) Similar presentation for somatosensory cortex (vS1) injection. (M-X) Comparisons of projections from different regions within S1. (M-N) M1 projections from fS1 (yellow) and orfS1 (green). (O-P) Injection sites. (Q-X) Striatal and entorhinal projections, with higher resolution images (U-X). Arrows show cell bodies; arrowheads show axonal projections.

Figure 3 | Topographic organization of contralateral cortical projections in frontal, motor, and somatosensory cortex
(A) Schematic illustrating how the corticocortical projections from two different injection sites are compared. The center of mass of cell bodies at the injection site is compared (offset distance in mm). The overlap of the ipsilateral of contralateral projections can be compared. (B) The correlation coefficient (PCC) for two example cases, comparing the suprathreshold voxel intensities for ipsilateral cortical projections. PCC=0.5372 for this example. (C) Sample coronal planes from two cases of aligned brains showing only suprathreshold ipsilateral cortical voxels. Spacing is ~0.75 mm along the anterior/posterior axis, from ~1.75 mm anterior to ~1.25 mm posterior. (D) Injection site locations in sensory, motor, and frontal locations. (E) Measurement of the total voxel intensity for ipsilateral cortical projections. Voxels range from 0-255 (in arbitrary units). Sensory injections were brighter than motor and frontal. Mean with SEM. 1 way ANOVA; df=2, F=4.89, p=0.00997. Tukey-corrected pairwise t-tests: Frontal–M1 (p=0.893), S1–M1 (p=0.035), S1–Frontal (p=0.015). (F) Ratio of voxel intensity for ipsilateral (injection site side) and contralateral voxels. 1 way ANOVA; df=2, F=12.07, p=2.66e-5. Tukey-corrected pairwise t-tests: Frontal–M1 (p=0.04), S1–M1 (p = 0.028), S1–Frontal (p = 0.000014). (G) Comparison of ipsilateral cortical correlations between injection sites for sensory, motor, and frontal injections. Mean with SEM. (H) Comparison of contralateral cortical correlations between injection sites for sensory, motor, and frontal injections. (I) Linear regression with 95% confidence interval. Two way ANCOVA examined the effects of region and ipsi/contra location on correlation (PCC) after controlling for distance (F(2,2165)=16.1, p=1.14e-7). Pairwise comparisons were computed and Bonferroni adjusted and all regions had significantly higher slopes for ipsi versus contra: S1 (F(2165)=9.87, adj. p=1.63e-22), M1 (F(1,867) = 13.8, p=2.12e-4), and Frontal (F(2165)=2.33, adj. p=2.01e-2).

Extended Data Figure 3 | Topographic organization of contralateral cortical projections in frontal, motor, and somatosensory cortex

(A) Comparison of ipsilateral (top row) and contralateral (bottom row) cortical correlations between injection sites for sensory, motor, and frontal injections. Subgroups within areas presented in different colors. Linear fit and 95% confidence interval (dotted line) plotted. (B) Comparison of ipsilateral (colors) and contralateral (gray) cortical correlations between injection sites for sensory, motor, and frontal injections. (C) Schematic of injection site locations. (D,E) Sum of ipsilateral voxel intensity by injection site location, with subdivision of cortical sites into finer divisions at bottom. (F,G) Ratio of contralateral to ipsilateral voxel intensity, with subdivision of cortical sites into finer divisions at bottom. (H,I) Overall correlation between ipsilateral and contralateral voxels by injection site, with subdivision of cortical sites into finer divisions at bottom.

Figure 4 | Area-by-area comparison of ipsi- and contralateral corticocortical projections in frontal, motor, and somatosensory cortex

(A) Schematic comparing corticocortical projections from a single injection site between ipsilateral and contralateral targets. (B) Average overall correlation (mean with SEM). (C-E). Sample coronal planes from aligned brains for somatosensory (C), motor (D), and frontal (E) injections. Left columns show ipsilateral cortex (injection side). Right columns show contralateral cortex, reflected for comparison. Only suprathreshold cortical voxels are shown. Spacing is ~0.75 mm along the anterior/posterior axis, from +1.75 mm anterior to -1.25 mm posterior. (F) Topographic areas of cortex in the Allen CCFv3. To compare contralateral cortical projections, homotypic projections are contralateral projections from one cortical area (the injection site) to the corresponding cortical area (dark green), while heterotopic projections (light green) target contralateral cortex in areas not corresponding to the injection site. (G-H) Quantification of the fraction of contralateral corticocortical projections to ipsi- and contralateral areas based on suprathreshold voxel intensity. All somatosensory (blue), motor (purple), and frontal (red) injections are combined. (I-K) Projection intensity to somatomotor cortical areas (per CCFv3) from somatosensory (blue), motor (purple), and frontal (red) injections. Regions are summed across cortical layers, noted on the x-axis in CCFv3 nomenclature. All areas are displayed for somatosensory cortex injections (I), with only somatomotor areas (J-K) displayed at right (where most axons are present). The summed intensity (in arbitrary units, AU) for suprathreshold voxels is plotted in (I) and (J). Solid lines are for ipsilateral projections and dotted lines are for contralateral injections. (K) represents peak normalized plots of the ipsilateral (solid) and contralateral (dotted) projection intensity. Ipsi- and contralateral intensity each normalized separately to compare the ipsi- and contralateral patterns in an intensity-independent manner.

Figure 5 | Symmetry of corticocortical projections in frontal, motor, and somatosensory cortex

(A-H) Injection sites in somatosensory (A-C), motor (D-F), and frontal (G-H) cortex, subdivided into topographic subregions (vS1, fS1, and orfS1 for somatosensory, A-C; vM1, fM1, llM1 for motor, D-F; and M2 and ALM for frontal, G-H). Injection sites are marked by red circles. Heatmap represents normalized projection intensity in ipsilateral cortex (summed across the dorsoventral axis), with contralateral intensity subtracted. Relative intensity is shown in the color map (yellow, stronger on the ipsilateral side; dark blue, stronger on the contralateral side). The outline of the dorsal surface of cortex is shown in (A). Black pixels represent values close to zero (contralateral and ipsilateral intensity roughly equal). (A-C) White arrowheads indicate strong ipsilateral connectivity with secondary somatosensory cortex (SSs). Red arrowheads indicate strong contralateral connectivity with entorhinal cortex. (D-F) Green arrowheads

indicate strong motor projections to ipsilateral somatosensory cortex (SSp-bfd). White arrowheads indicate strong ipsilateral connectivity with secondary somatosensory cortex (SSs). (G-H) White arrowheads indicate strong ipsilateral connectivity with primary motor cortex (MOp). (I-K) Projection intensity to all cortical areas (per CCFv3) from subregions of somatosensory cortex injections. Left plot (I and J) shows the summed intensity (in arbitrary units, AU) for suprathreshold voxels in ipsilateral cortex for each individual case (color coded to the subregion), with arrow at top indicating the CCFv3 region best corresponding to the injection site. The right plot shows the same data for the contralateral side. The mean of the ipsilateral (left) and contralateral (right) is presented in (J). Normalized plots of ipsilateral (blue colors) and contralateral (black) are presented in (K) for vS1 (left), fS1 (middle), and orfS1 (right). (L) Color coded plot of the CCFv3 areas for somatosensory cortex.

Figure 6 | Ipsi- and contralateral corticostriatal projections of IT-type neurons in frontal, motor, and somatosensory cortex

(A-I) Coronal images showing injection site of AAV-DIO-XFP into frontal cortex (A-C), motor cotex (D-F), and somatosensory cortex (G-I). Left column shows ipsilateral side, right column shows contralateral side, with reflected image shown for comparison. (J-T) More detailed presentation of the injection sites in ALM (J, green) and M2 (K, red) and their striatal targets. Arrowheads show axonal projections. (L-N) present the overall difference in striatal axonal intensity between ipsilateral and contralateral projections (see Fig. 8) for the ALM (L) and M2 (M) injections, with a schematic of the dorsal view of striatum (Str). Red lines indicate approximate planes of the images in (O-T), with the striatum boxed in the corresponding color.

Figure 7 | Topographic organization of contralateral corticostriatal projections in frontal, motor, and somatosensory cortex

(A) Schematic illustrating how the corticostriatal projections from two different injection sites are compared. The center of mass of cell bodies at the injection site is compared (offset distance in mm). The overlap of the ipsilateral of contralateral projections can be compared. (B) The correlation coefficient (PCC) for two example cases, comparing the suprathreshold voxel intensities for ipsilateral striatal projections. PCC=0.4693 for this frontal example. (C) Sample coronal planes from two cases of aligned brains showing only suprathreshold contralateral striatal voxels. Spacing is ~0.75 mm along the anterior/posterior axis, from ~1.50 mm anterior to ~1.50 mm posterior. (D) Injection site locations in sensory, motor, and frontal locations. (E) Measurement of the total voxel intensity for ipsilateral striatal projections. Voxels range from 0-255 (in arbitrary units). Frontal injections were brighter than somatosensory and motor. Mean with SEM. 1 way ANOVA; df=2, F=13.63, p=8.21e-6. Tukey-corrected pairwise t-tests: Frontal–M1 (p=1.5e-4), S1–M1 (p=0.787), S1–Frontal (p=2.1e-5). (F) Ratio of voxel intensity for ipsilateral (injection site side) and contralateral voxels. 1 way ANOVA; df=2, F=32.84, p=4.18e-11. Tukey-corrected pairwise t-tests: Frontal–M1 (p=1.0e-6), S1–M1 (p=0.03), S1–Frontal (p<1e-16). (G) Comparison of ipsilateral striatal correlations between injection sites for sensory, motor, and frontal injections. (H) Comparison of contralateral striatal correlations between injection sites for sensory, motor, and frontal injections. (I) Linear regression with 95% confidence interval. Two way ANCOVA examined the effects of region and ipsi/contra location on correlation (PCC) after controlling for distance (F(2,2165)= 67,565, p=3.45e-29). Pairwise comparisons were computed and Bonferroni adjusted and all regions had significantly higher slopes for ipsi versus contra: S1 (F(2162)=16.7, adj. p=3.46e-59), M1 (F(2162)=6.46, adj. p=1.3e-10), and Frontal (F(2162)=2.33, adj. p=0.91).

Extended Data Figure 7 | Topographic organization of ipsi- and contralateral corticostriatal projections

(A) Comparison of ipsilateral (top row) and contralateral (bottom row) corticostriatal correlations between injection sites for sensory, motor, and frontal injections. Subgroups within areas presented in different colors. Linear fit and 95% confidence interval (dotted line) plotted. (B) Comparison of ipsilateral (colors) and contralateral (gray) corticostriatal correlations between injection sites for sensory, motor, and frontal injections. (C) Schematic of injection site locations. (D,E) Sum of ipsilateral voxel intensity by injection site location, with subdivision into finer divisions by injection site at bottom. (F,G) Ratio of contralateral to ipsilateral voxel intensity, with subdivision into finer divisions by injection site at bottom. (H,I) Overall correlation between ipsilateral and contralateral voxels by injection site, with subdivision into finer divisions by injection site at bottom.

Figure 8 | Symmetry of corticostriatal projections from frontal, motor, and somatosensory cortex

(A-H) Striatal projections from injection sites in somatosensory (A-C), motor (D-F), and frontal (G-H) cortex, subdivided into topographic subregions (vS1, fS1, and orfS1 for somatosensory, A-C; vM1, fM1, llM1 for motor, D-F; and M2 and ALM for frontal, G-H). Injection sites are not marked. Heatmap represents normalized projection intensity in ipsilateral striatum (summed across the dorsoventral axis), with contralateral intensity subtracted. Black pixels represent values close to zero (contralateral and ipsilateral intensity roughly equal), with yellow representing sites with stronger ipsilateral strength (injection sites) and dark blue voxels representing stronger contralateral sites. White arrowheads reflect anterolateral sites of strong contralateral connectivity. Schematic inset at bottom right shows the shape of striatum as viewed from the dorsal side, with midline and anterior/posterior axis labeled.

References

Alexander, G.E., DeLong, M.R., and Strick, P.L. (1986). Parallel organization of functionally segregated circuits linking basal ganglia and cortex. Annu Rev Neurosci *9*, 357-381.

Alloway, K.D., Lou, L., Nwabueze-Ogbo, F., and Chakrabarti, S. (2006). Topography of cortical projections to the dorsolateral neostriatum in rats: multiple overlapping sensorimotor pathways. J Comp Neurol *499*, 33-48.

Alloway, K.D., Mutic, J.J., Hoffer, Z.S., and Hoover, J.E. (2000). Overlapping corticostriatal projections from the rodent vibrissal representations in primary and secondary somatosensory cortex. J Comp Neurol *426*, 51-67.

Bohland, J.W., Wu, C., Barbas, H., Bokil, H., Bota, M., Breiter, H.C., Cline, H.T., Doyle, J.C., Freed, P.J., Greenspan, R.J., et al. (2009). A proposal for a coordinated effort for the determination of brainwide neuroanatomical connectivity in model organisms at a mesoscopic scale. PLoS Comput Biol *5*, e1000334. 10.1371/journal.pcbi.1000334.

Borra, E., Biancheri, D., Rizzo, M., Leonardi, F., and Luppino, G. (2022). Crossed Corticostriatal Projections in the Macaque Brain. J Neurosci *42*, 7060-7076.

Brecht, M., Krauss, A., Muhammad, S., Sinai-Esfahani, L., Bellanca, S., and Margrie, T.W. (2004). Organization of rat vibrissa motor cortex and adjacent areas according to cytoarchitectonics, microstimulation, and intracellular stimulation of identified cells. J Comp Neurol *479*, 360-373.

Brown, S.P., and Hestrin, S. (2009). Intracortical circuits of pyramidal neurons reflect their long-range axonal targets. Nature *457*, 1133-1136.

Carvell, G.E., and Simons, D.J. (1986). Somatotopic organization of the second somatosensory area (SII) in the cerebral cortex of the mouse. Somatosens Res *3*, 213-237.

Cavada, C., and Goldman-Rakic, P.S. (1991). Topographic segregation of corticostriatal projections from posterior parietal subdivisions in the macaque monkey. Neuroscience *42*, 683-696.

Choi, E.Y., Tanimura, Y., Vage, P.R., Yates, E.H., and Haber, S.N. (2017). Convergence of prefrontal and parietal anatomical projections in a connectional hub in the striatum. Neuroimage *146*, 821-832.

Deemyad, T., Puig, S., Papale, A.E., Qi, H., LaRocca, G.M., Aravind, D., LaNoce, E., and Urban, N.N. (2022). Lateralized Decrease of Parvalbumin+ Cells in the Somatosensory Cortex of ASD Models Is Correlated with Unilateral Tactile Hypersensitivity. Cereb Cortex *32*, 554-568.

Drager, U.C. (1975). Receptive fields of single cells and topography in mouse visual cortex. J Comp Neurol *160*, 269-290.

Eastwood, B.S., Hooks, B.M., Paletzki, R.F., O'Connor, N.J., Glaser, J.R., and Gerfen, C.R. (2019). Whole mouse brain reconstruction and registration to a reference atlas with standard histochemical processing of coronal sections. J Comp Neurol *527*, 2170-2178.

Economo, M.N., Clack, N.G., Lavis, L.D., Gerfen, C.R., Svoboda, K., Myers, E.W., and Chandrashekar, J. (2016). A platform for brain-wide imaging and reconstruction of individual neurons. Elife *5*. 10.7554/eLife.10566.

Felleman, D.J., and Van Essen, D.C. (1991). Distributed hierarchical processing in the primate cerebral cortex. Cereb Cortex *1*, 1-47.

Foster, N.N., Barry, J., Korobkova, L., Garcia, L., Gao, L., Becerra, M., Sherafat, Y., Peng, B., Li, X., Choi, J.H., et al. (2021). The mouse cortico-basal ganglia-thalamic network. Nature *598*, 188-194.

Gerbella, M., Borra, E., Mangiaracina, C., Rozzi, S., and Luppino, G. (2016). Corticostriate Projections from Areas of the "Lateral Grasping Network": Evidence for Multiple Hand-Related Input Channels. Cereb Cortex *26*, 3096-3115.

Gerfen, C.R., Paletzki, R., and Heintz, N. (2013). GENSAT BAC cre-recombinase driver lines to study the functional organization of cerebral cortical and basal ganglia circuits. Neuron *80*, 1368-1383.

Griggs, W.S., Kim, H.F., Ghazizadeh, A., Costello, M.G., Wall, K.M., and Hikosaka, O. (2017). Flexible and Stable Value Coding Areas in Caudate Head and Tail Receive Anatomically Distinct Cortical and Subcortical Inputs. Front Neuroanat *11*, 106.

Guo, Z.V., Li, N., Huber, D., Ophir, E., Gutnisky , D.A., Ting, J.T., Feng, G., and Svoboda, K. (2014). Flow of cortical activity underlying a tactile decision in mice. Neuron *81*, 179-194.

Haber, S.N. (2003). The primate basal ganglia: parallel and integrative networks. J Chem Neuroanat *26*, 317-330.

Hintiryan, H., Foster, N.N., Bowman, I., Bay, M., Song, M.Y., Gou, L., Yamashita, S., Bienkowski, M.S., Zingg, B., Zhu, M., et al. (2016). The mouse cortico-striatal projectome. Nat Neurosci *19*, 1100-1114.

Histed, M.H., Ni, A.M., and Maunsell, J.H. (2012). Insights into cortical mechanisms of behavior from microstimulation experiments. Progress in neurobiology. 10.1016/j.pneurobio.2012.01.006.

Hoffer, Z.S., Hoover, J.E., and Alloway, K.D. (2003). Sensorimotor corticocortical projections from rat barrel cortex have an anisotropic organization that facilitates integration of inputs from whiskers in the same row. J Comp Neurol *466*, 525-544.

Hooks, B.M. (2017). Sensorimotor Convergence in Circuitry of the Motor Cortex. Neuroscientist *23*, 251-263.

Hooks, B.M., Hires, S.A., Zhang, Y.X., Huber, D., Petreanu, L., Svoboda, K., and Shepherd, G.M. (2011). Laminar analysis of excitatory local circuits in vibrissal motor and sensory cortical areas. PLoS Biol *9*, e1000572. 10.1371/journal.pbio.1000572.

Hooks, B.M., Mao, T., Gutnisky, D.A., Yamawaki, N., Svoboda, K., and Shepherd, G.M. (2013). Organization of cortical and thalamic input to pyramidal neurons in mouse motor cortex. J Neurosci *33*, 748-760.

913 Hooks, B.M., Papale, A.E., Paletzki, R.F., Feroze, M.W., Eastwood, B.S., Couey, J.J.,
914 Winnubst, J., Chandrashekar, J., and Gerfen, C.R. (2018). Topographic precision in sensory
915 and motor corticostriatal projections varies across cell type and cortical area. Nat Commun *9*,
916 3549. 10.1038/s41467-018-05780-7.
917
918 Jarbo, K., and Verstynen, T.D. (2015). Converging structural and functional connectivity of
919 orbitofrontal, dorsolateral prefrontal, and posterior parietal cortex in the human striatum. J
920 Neurosci *35*, 3865-3878.
921
922 Johansson, Y., and Silberberg, G. (2020). The Functional Organization of Cortical and Thalamic
923 Inputs onto Five Types of Striatal Neurons Is Determined by Source and Target Cell Identities.
924 Cell Rep *30*, 1178-1194 e1173.
925
926 Jones, E.G., Coulter, J.D., Burton, H., and Porter, R. (1977). Cells of origin and terminal
927 distribution of corticostriatal fibers arising in the sensory-motor cortex of monkeys. J Comp
928 Neurol *173*, 53-80.
929
930 Komiyama, T., Sato, T.R., O'Connor, D.H., Zhang, Y.X., Huber, D., Hooks, B.M., Gabitto, M.,
931 and Svoboda, K. (2010). Learning-related fine-scale specificity imaged in motor cortex circuits of
932 behaving mice. Nature *464*, 1182-1186.
933
934 Kuan, L., Li, Y., Lau, C., Feng, D., Bernard, A., Sunkin, S.M., Zeng, H., Dang, C., Hawrylycz, M.,
935 and Ng, L. (2015). Neuroinformatics of the Allen Mouse Brain Connectivity Atlas. Methods *73*, 4-
936 17.
937
938 Kunzle, H. (1975). Bilateral projections from precentral motor cortex to the putamen and other
939 parts of the basal ganglia. An autoradiographic study in Macaca fascicularis. Brain Res *88*, 195-
940 209.
941
942 Lee, J., Wang, W., and Sabatini, B.L. (2020). Anatomically segregated basal ganglia pathways
943 allow parallel behavioral modulation. Nat Neurosci *23*, 1388-1398.
944
945 Li, C.X., and Waters, R.S. (1991). Organization of the mouse motor cortex studied by retrograde
946 tracing and intracortical microstimulation (ICMS) mapping. Can J Neurol Sci *18*, 28-38.
947
948 Li, N., Daie, K., Svoboda, K., and Druckmann, S. (2016). Robust neuronal dynamics in premotor
949 cortex during motor planning. Nature *532*, 459-464.
950
951 Mao, T., Kusefoglu, D., Hooks, B.M., Huber, D., Petreanu, L., and Svoboda, K. (2011). Long-
952 range neuronal circuits underlying the interaction between sensory and motor cortex. Neuron
953 *72*, 111-123.
954
955 McGeorge, A.J., and Faull, R.L. (1989). The organization of the projection from the cerebral
956 cortex to the striatum in the rat. Neuroscience *29*, 503-537.
957
958 McGuire, P.K., Bates, J.F., and Goldman-Rakic, P.S. (1991a). Interhemispheric integration: I.
959 Symmetry and convergence of the corticocortical connections of the left and the right principal
960 sulcus (PS) and the left and the right supplementary motor area (SMA) in the rhesus monkey.
961 Cereb Cortex *1*, 390-407.
962

McGuire, P.K., Bates, J.F., and Goldman-Rakic, P.S. (1991b). Interhemispheric integration: II. Symmetry and convergence of the corticostriatal projections of the left and the right principal sulcus (PS) and the left and the right supplementary motor area (SMA) of the rhesus monkey. Cereb Cortex *1*, 408-417.

Merzenich, M.M., and Brugge, J.F. (1973). Representation of the cochlear partition of the superior temporal plane of the macaque monkey. Brain Res *50*, 275-296.

Middleton, F.A., and Strick, P.L. (2000). Basal ganglia and cerebellar loops: motor and cognitive circuits. Brain Res Brain Res Rev *31*, 236-250.

Morel, A., Garraghty, P.E., and Kaas, J.H. (1993). Tonotopic organization, architectonic fields, and connections of auditory cortex in macaque monkeys. J Comp Neurol *335*, 437-459.

Oh, S.W., Harris, J.A., Ng, L., Winslow, B., Cain, N., Mihalas, S., Wang, Q., Lau, C., Kuan, L., Henry, A.M., et al. (2014). A mesoscale connectome of the mouse brain. Nature *508*, 207-214.

Paletzki, R., and Gerfen, C.R. (2015). Whole Mouse Brain Image Reconstruction from Serial Coronal Sections Using FIJI (ImageJ). Curr Protoc Neurosci *73*, 1 25 21-21.

Paxinos, G., and Franklin, H.B.J. (2004). The Mouse Brain in Stereotaxic Coordinates: Compact Second Edition (Elsevier).

Penfield, W., and Boldery, P. (1937). Somatic motor and sensory representation in the cerebral cortex of man as studied by electrical stimulation. Brain *60*, 389–443.

Petreanu, L., Huber, D., Sobczyk, A., and Svoboda, K. (2007). Channelrhodopsin-2-assisted circuit mapping of long-range callosal projections. Nat Neurosci *10*, 663-668.

Petrus, E., Dembling, S., Usdin, T., Isaac, J.T.R., and Koretsky, A.P. (2020). Circuit-Specific Plasticity of Callosal Inputs Underlies Cortical Takeover. J Neurosci *40*, 7714-7723.

Petrus, E., Saar, G., Ma, Z., Dodd, S., Isaac, J.T.R., and Koretsky, A.P. (2019). Interhemispheric plasticity is mediated by maximal potentiation of callosal inputs. Proc Natl Acad Sci U S A *116*, 6391-6396.

Reig, R., and Silberberg, G. (2016). Distinct Corticostriatal and Intracortical Pathways Mediate Bilateral Sensory Responses in the Striatum. Cereb Cortex *26*, 4405-4415.

Rocco-Donovan, M., Ramos, R.L., Giraldo, S., and Brumberg, J.C. (2011). Characteristics of synaptic connections between rodent primary somatosensory and motor cortices. Somatosens Mot Res *28*, 63-72.

Selemon, L.D., and Goldman-Rakic, P.S. (1985). Longitudinal topography and interdigitation of corticostriatal projections in the rhesus monkey. J Neurosci *5*, 776-794.

Szczupak, D., Iack, P.M., Rayee, D., Liu, C., Lent, R., Tovar-Moll, F., and Silva, A.C. (2023). The relevance of heterotopic callosal fibers to interhemispheric connectivity of the mammalian brain. Cereb Cortex *33*, 4752-4760.

1013 Tappan, S.J., Eastwood, B.S., O'Connor, N., Wang, Q., Ng, L., Feng, D., Hooks, B.M., Gerfen,
1014 C.R., Hof, P.R., Schmitz, C., and Glaser, J.R. (2019). Automatic navigation system for the
1015 mouse brain. J Comp Neurol *527*, 2200-2211.
1016
1017 Tennant, K.A., Adkins, D.L., Donlan, N.A., Asay, A.L., Thomas, N., Kleim, J.A., and Jones, T.A.
1018 (2011). The organization of the forelimb representation of the C57BL/6 mouse motor cortex as
1019 defined by intracortical microstimulation and cytoarchitecture. Cereb Cortex *21*, 865-876.
1020
1021 Viswanathan, S., Williams, M.E., Bloss, E.B., Stasevich, T.J., Speer, C.M., Nern, A., Pfeiffer,
1022 B.D., Hooks, B.M., Li, W.P., English, B.P., et al. (2015). High-performance probes for light and
1023 electron microscopy. Nat Methods *12*, 568-576.
1024
1025 Wall, N.R., De La Parra, M., Callaway, E.M., and Kreitzer, A.C. (2013). Differential innervation
1026 of direct- and indirect-pathway striatal projection neurons. Neuron *79*, 347-360.
1027
1028 Wang, Q., and Burkhalter, A. (2007). Area map of mouse visual cortex. J Comp Neurol *502*,
1029 339-357.
1030
1031 Wang, Q., Ding, S.L., Li, Y., Royall, J., Feng, D., Lesnar, P., Graddis, N., Naeemi, M., Facer, B.,
1032 Ho, A., et al. (2020). The Allen Mouse Brain Common Coordinate Framework: A 3D Reference
1033 Atlas. Cell *181*, 936-953 e920.
1034
1035 Winnubst, J., Bas, E., Ferreira, T.A., Wu, Z., Economo, M.N., Edson, P., Arthur, B.J., Bruns, C.,
1036 Rokicki, K., Schauder, D., et al. (2019). Reconstruction of 1,000 Projection Neurons Reveals
1037 New Cell Types and Organization of Long-Range Connectivity in the Mouse Brain. Cell *179*,
1038 268-281 e213.
1039
1040 York, G.K., 3rd, and Steinberg, D.A. (2011). Hughlings Jackson's neurological ideas. Brain *134*,
1041 3106-3113.
1042
1043 Zingg, B., Hintiryan, H., Gou, L., Song, M.Y., Bay, M., Bienkowski, M.S., Foster, N.N.,
1044 Yamashita, S., Bowman, I., Toga, A.W., and Dong, H.W. (2014). Neural networks of the mouse
1045 neocortex. Cell *156*, 1096-1111.